Published in "Galactic and Extragalactic Radio Astronomy", 1988, 2nd edition, eds. G.L. Verschuur and K.I. Kellermann.

15. RADIO SOURCES AND COSMOLOGY

James J. Condon

Table of Contents

15.1. INTRODUCTION

Since the realization in the 1950s that the majority of catalogued radio sources are extragalactic and that some of the strongest are at cosmological distances, the application of radio observations to cosmological studies has been a central theme in radio astronomy.

The ratios of flux density to luminosity and angular size to projected linear size at different redshifts can, in principle, distinguish between world models by their geometrical properties and measure directly such basic parameters as the Hubble constant H_0 and the deceleration parameter q_0. The sensitivity and resolution of modern radio telescopes are more than adequate to make such measurements on a variety of sources, even at redshifts $z >> 1$. Unfortunately, no "standard candle" or "standard rod" sources with luminosities or linear sizes known in a model-independent way have yet been recognized. Not only do the luminosities and sizes of extragalactic radio sources cover a wide range, but also their median values in radio-source populations evolve with cosmological epoch.

A less direct, but so far more successful, approach is to obtain complete samples of radio sources and model statistics describing radio-source populations. For example, the flux-density distribution of sources led to the discovery of evolution on cosmological time scales and the rejection of the steady-state world model. Such cosmological studies of radio-source populations might be used to constrain astrophysical theories of radio sources, their parent galaxies, their environments, and their evolution. Radio-selected samples are particularly well suited to these cosmological investigations for several reasons. Modern radio surveys are statistically complete and quite reliable, and radio flux densities are routinely measured with high accuracy. Radio samples are not badly confused by galactic stars, and they are not affected by dust obscuration in our galaxy, intervening material at high redshifts, or the host galaxies of the sources themselves (Ostriker and Heisler 1984). Radio sources have fairly smooth power law spectra, so there is no sharp redshift cutoff or discrimination against sources in certain redshift bands. Finally, many radio sources that have been found at redshifts $z \approx 1$ are so luminous that they could easily be detected in moderately sensitive surveys even at very high redshifts ($z \approx 10$). The biggest limitation of radio-selected samples is their dependence on optical identifications and spectroscopy for information about distance and host-galaxy morphology (elliptical galaxy, spiral galaxy, quasar, etc.). Only for the $N \approx 200$ strongest radio sources are the optical identifications and spectroscopy complete. The redshift distributions of most faint sources can only be estimated with the aid of evolutionary models constrained by statistical data - source counts, angular-size distributions, etc. This chapter describes some of the tests of world models and cosmological evolution that can be made using discrete radio sources.

15.2. BASIC RELATIONS

The flux density S as a function of frequency ν and the angular size θ of a radio source are the observables directly relevant to most cosmological problems. They are related to the intrinsic source luminosity L and projected linear size d as described below.

Consider an isotropic source at redshift z with spectral luminosity L at frequency ν (measured in the source frame). Its spectral flux density S measured at the same frequency ν (in the observer's frame) will be

$$S = \frac{L}{A(1+z)^{1+\alpha}}, \tag{15.1}$$

where A is the area of the sphere centered on the source and containing the observer and $\alpha \equiv -\ln(S / S_0) / \ln(\nu / \nu_0)$ is the two-point spectral index between the frequencies ν and $\nu_0 = \nu / (1 + z)$ in the observer's frame. (Note that the *negative* sign convention for α is used throughout this chapter.) The $(1 + z)^{1+\alpha}$ term expresses the special relativistic Doppler correction; the geometry and expansion dynamics of the universe appear only in A. An "effective distance" D (Longair 1978) can be defined by $A \equiv 4\pi D^2$. Since the area of the sphere centered on the observer and containing a source at redshift z is always $A / (1 + z)^2$, the relation between (projected) linear size d and measured angular size θ is

$$\theta = \frac{d(1+z)}{D} \tag{15.2}$$

The "angular size" distance is defined by $D_\theta \equiv d / \theta = D / (1 + z)$. The "bolometric luminosity distance" D_{bol} defined by $S_{bol} = L_{bol} / (4\pi D_{bol}^2)$ is given by $D_{bol} = D(1 + z)$.

In Friedmann models (cosmological constant $\Lambda = 0$) with zero pressure, density parameter $\Omega = 2q_0$, and current Hubble parameter H_0 the effective distance is traditionally given (Mattig 1958) as

$$D = \frac{2c\{\Omega z + (\Omega - 2)[(1+\Omega z)^{1/2} - 1]\}}{H_0 \Omega^2 (1+z)}. \tag{15.3}$$

However, this formula is numerically unstable for small Ωz, the transformation (based on Terrell 1977)

$$D = \left(\frac{cz}{H_0}\right)\left(\frac{1}{1+z}\right)\left[1 + \frac{z(1-\Omega/2)}{(1+\Omega z)^{1/2} + 1 + \Omega z/2}\right] \tag{15.4}$$

is better for numerical calculations. For particular values of Ω, D reduces to the simpler forms:

$$D = \frac{cz}{H_0}\left(\frac{1+z/2}{1+z}\right) \qquad (\Omega = 0) \tag{15.5a}$$

$$D = \frac{2c}{H_0}[1-(1+z)^{-1/2}] \qquad (\Omega = 1) \tag{15.5b}$$

$$D = \frac{cz}{H_0(1+z)} \qquad (\Omega = 2). \tag{15.5c}$$

To describe the distributions of sources in space and time, we also need the comoving volume dV of the spherical shell extending from z to $z + dz$. It is $dV = 4\pi D^2 dr$, where the comoving radial coordinate element is $dr = -(1 + z)c\,dt$. In a Friedmann universe the expansion rate is

$$\frac{dz}{dt} = -H_0(1+z)^2(1+\Omega z)^{1/2} \tag{15.6}$$

so

$$dV = \frac{4\pi D^2 c\,dz}{H_0(1+z)(1+\Omega z)^{1/2}}. \tag{15.7}$$

15.3. THE "WORLD PICTURE" AND SOURCE EVOLUTION

The interval during which radio observations have been made is much shorter than the active lifetimes of individual sources and the time scales on which populations of radio sources evolve, so at best the data can give only a "world picture" covering the surface of our past light cone. The luminosity functions, size distributions, etc. of different source populations at different lookback times can be compared to reveal evolution, but we cannot directly observe any changes actually taking place. One consequence of this limitation is illustrated by Figure 15.1, showing the radio luminosity functions of elliptical galaxies at two different epochs. The luminosity functions do not overlap, so cosmological evolution must occur. The arrows in Figure 15.1(a) indicate one way in which the data might be interpreted - the comoving density ρ_m of sources was higher in the past, with the greatest changes being experienced by the most luminous sources. Such evolution is called "luminosity-dependent density evolution," a term that suggests an evolutionary mechanism capable of distinguishing between weak and strong sources. The arrows in Figure 15.1(b) show a very different interpretation of the *same* two luminosity functions - the luminosities of *all* sources were higher in the past, by an amount independent of luminosity. This "luminosity evolution" interpretation is consistent with evolutionary mechanisms that affect weak and strong sources alike. Since the active lifetimes of individual radio sources are generally shorter than the evolutionary time scales, which are, in turn, shorter than the ages of elliptical

galaxies, descriptions of evolution based on associating points or features in the luminosity functions from different epochs probably oversimplify the actual changes occurring on the individual source level. In any case, the data cannot distinguish between them.

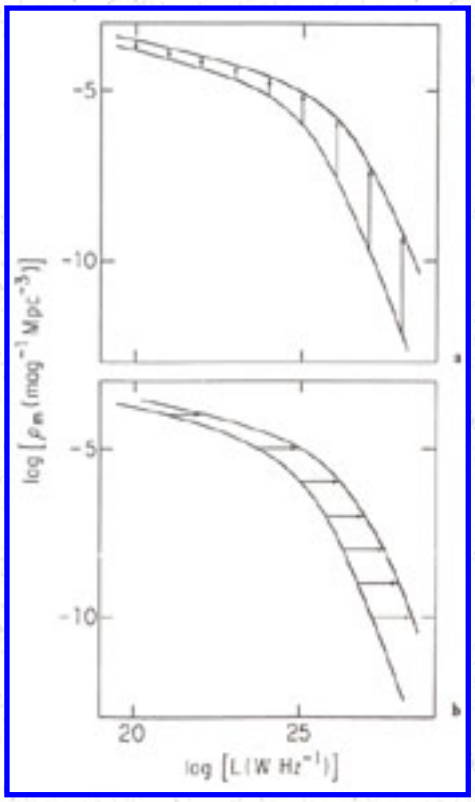

Figure 15.1. The 1.4-GHz luminosity functions of elliptical radio galaxies at $z = 0$ and $z = 0.8$ with arrows illustrating (a) luminosity-dependent density evolution and (b) pure luminosity evolution. These particular luminosity functions are from the "shell model" described in Section 15.9. Abscissas: log luminosity (W Hz^{-1}). Ordinates: log comoving density (mag^{-1} Mpc^{-3}).

Because luminosity functions $\rho_m(L \mid z)$ have dimensions of comoving source density, evolution has historically been described in terms of density changes. The "evolution function"

$$E(L, z) \equiv \frac{\rho_m(L|z)}{\rho_m(L|z = 0)} \tag{15.8}$$

is an example. Consequently, there is a widespread misconception that the data *imply* "luminosity-dependent density evolution," leading to unjustified conclusions like "In view of the lack of evolution of

the low-luminosity sources, it seems implausible that their spectra should change with redshift." Even though the evolution function completely specifies the changes of mean source density with luminosity and epoch, it cannot completely describe the course of evolution.

Existing data do not even determine our world picture completely. The "generalized luminosity function" $\rho_m(L, \alpha, ... | z, \nu)$ of sources with luminosity L, spectral index α, and other relevant properties (e.g., type of galaxy) indicated by ... at redshift z and frequency ν is only partially determined. Most sources in the flux-limited sample found by any single radio survey complete to some level S are confined to a narrow diagonal band in the luminosity-redshift plane (Figure 15.2). Known radio sources span ten decades in luminosity and five in redshift, so surveys with a wide range of limiting flux densities S made with a number of different radio telescopes are needed to fill in the (L, z)-plane. More difficult than this is obtaining the optical identifications and redshifts needed to locate individual sources on the (L, z)-plane. Spectroscopic redshifts are available for most sources with $S \geq 2$ Jy at $\nu = 1.4$ GHz, but fainter sources with known S and unknown z could lie almost anywhere on the diagonal lines of constant S. The Leiden-Berkeley Deep Survey (Windhorst 1984, Windhorst et al. 1984b, Kron et al. 1985, Windhorst et al. 1985) is a major project to find sources as faint as $S \approx 1$ mJy at $\nu = 1.4$ GHz, identify nearly all of them on very deep photographic plates or CCD images and obtain photometric or spectroscopic redshifts. Efforts like this should eventually yield a *direct* determination of the generalized luminosity function, but until then we are limited to making models that use known radio sources with only weak constraints on their redshift distributions to extrapolate into unknown regions of the (L, z)-plane. The available data are presented in Section 15.4 and some models in Section 15.5.

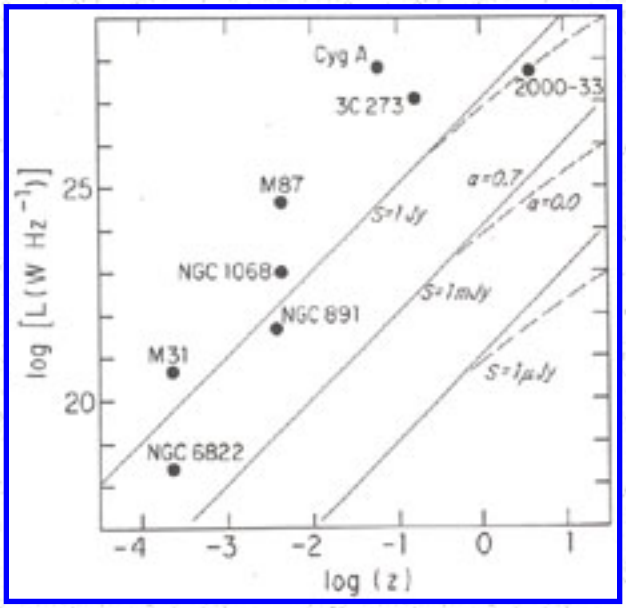

Figure 15.2. Luminosities and redshifts of representative radio sources found at ν = 1.4 GHz. Most nearby sources with $L < 10^{23}$ W Hz^{-1} are associated with spiral galaxies. The faintest are found in dwarf irregulars like NGC 6822; the luminosity of M31 is typical for full-sized spiral galaxies. An unusually high star formation rate probably accounts for the relatively high radio luminosity of NGC 891, and the Seyfert/starburst galaxy NGC 1068 is the strongest radio emitter of the nearby spiral galaxies. Elliptical galaxies such as M87 dominate the radio-source population at higher powers, reaching $L \approx 10^{28}$ W Hz^{-1}). in the case of Cygnus A. Radio-selected quasars are concentrated near the upper end of this luminosity range and have known redshifts between z = 0.158 (3C273) and z = 3.78 (2000-33). Lines of constant flux density are shown for sources with spectral indices α = 0.7 (solid lines) and α = 0.0 (broken curves) in an Einstein-de Sitter universe (Ω = 1) with H_0 = 100 km s^{-1} Mpc^{-1}. Nearly all radio galaxies selected at ν = 1.4 GHz have spectral indices near α = 0.7, while many quasars have $\alpha \approx 0$. The faintest discrete sources detected at ν = 1.4 GHz have flux densities $S \approx 100$ μJy and the sky density of sources as faint as $S \approx 10$ μJy has been estimated statistically. Abscissa: log redshift. Ordinate: log spectral luminosity (W Hz^{-1}).

15.4. SOURCE POPULATION DATA

15.4.1. The Local Luminosity Function

The simplest form of the radio luminosity function $\rho_m(L \mid z, \nu)$ specifies the comoving space density of

all sources per unit of $\log_m(L)$ [often $m \equiv \mathrm{dex}(0.4) = 1$ "magnitude"] in luminosity L at frequency ν (in the source frame) and redshift z. The vertical bar notation is used to distinguish distribution variables from parameters. The "local" luminosity function $\rho_m(L|\, z = 0, \nu)$ of low-luminosity sources can be obtained directly from flux-limited radio observations of nearby galaxies in optically complete samples. Let V_m be the maximum volume in which an optically selected galaxy would be brighter than both the radio flux density-and optical magnitude limits. If the sample galaxies are distributed uniformly in space, the density contributed by the N radio-detected galaxies with luminosities in the luminosity bin of width m centered on L is

$$\rho_m(L|z=0,\nu) = \sum_{i=1}^{N} \left(\frac{1}{V_m}\right)_i \tag{15.9}$$

with an rms statistical uncertainty

$$\sigma = \left[\sum_{i=1}^{N} \left(\frac{1}{V_m}\right)_i^2\right]^{1/2} \tag{15.10}$$

The actual errors in ρ_m, are larger at the lowest luminosities because clustering in the accessible volumes V_m associated with intrinsically faint galaxies is significant. Since radio sources of intermediate luminosities have space densities too low for them to be numerous in the small volumes covered by most optically complete samples, sources identified with bright low-redshift galaxies found in complete radio surveys must be used (e.g., Auriemma et al. 1977).

At the very highest luminosities the source density is so low that the nearest sources are already at cosmological distances and lookback times affected by evolution; their "local" luminosity function can only be estimated with the aid of evolutionary models. The density of evolving sources is uniform in volume elements dV' that have been weighted by the evolution function $E(L, z)$ (Equation 15.8). The weighted volume V'_m replacing V_m in Equation (15.9) is

$$V'_m = \int_0^{z_m} E(L,z)\,dV \tag{15.11}$$

for a source of luminosity L that could be seen out to a redshift z_m.

The distribution of

$$\frac{V}{V_m} \equiv \frac{\int_0^z dV}{\int_0^{z_m} dV} \qquad (15.12)$$

should be uniform in the interval (0,1) if the sources in any sample have a constant (comoving) density (cf. Schmidt 1968). Incompleteness is usually revealed by a deficit of V / V_m values near unity, and monotonically increasing evolution by $\langle V / V_m \rangle > 0.5$ for the whole sample.

The local luminosity function is best determined at ν = 1.4 GHz. The local luminosity function of spiral galaxies has recently been derived from sensitive VLA observations (Condon 1987) of all spirals north of δ = - 45° and brighter than B_T = + 12 mag, the completeness limit of the *Revised Shapley-Ames Catalog* (Sandage and Tammann 1981). The corresponding luminosity function for low-redshift E and SO galaxies was obtained by Auriemma et al. (1977) from both optical and radio samples as described above. There are essentially no local radio-selected quasars. The contributions of Seyfert galaxies and optically selected quasars to the local luminosity function fall within the high-luminosity extension of the spiral galaxy component (Meurs and Wilson 1984), and the radio-loud quasars are presumed to be in elliptical galaxies. The resulting 1.4-GHz local luminosity function $\rho_m(L \mid z = 0, \nu = 1.4 \text{ GHz})$ is plotted in Figure 15.3(a) for a Hubble parameter H_0 = 100 km s^{-1} Mpc^{-1} (the value used throughout this chapter).

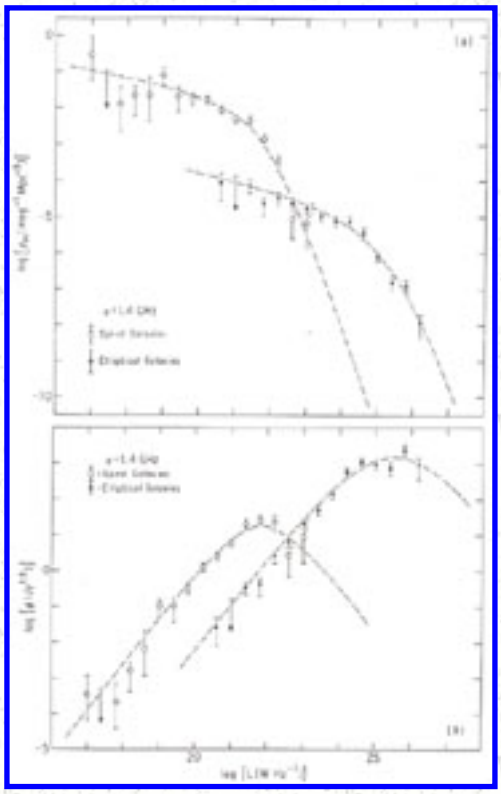

Figure 15.3. (a) Local luminosity function $\rho_m(L \mid z = 0, \nu = 1.4\ \mathrm{GHz})$. Open circles represent radio sources associated with spiral galaxies (Condon 1987), and the filled circles are based on the Auriemma et al. (1977) luminosity function for E and S0 galaxies. Abscissa: log luminosity (W Hz^{-1}). Ordinate: log comoving density (mag^{-1} Mpc^{-3}). (b) Local weighted luminosity function $\phi(L \mid z) = 0, \nu = 1.4\ \mathrm{GHz})$. Abscissa: log luminosity (W Hz^{-1}). Ordinate: log weighted luminosity function ($\mathrm{Jy}^{1.5}$).

Other forms of the luminosity function are sometimes useful. One is the co-moving density $\rho(L \mid z, \nu)\ dL$ of sources with luminosities L to $L + dL$ Since $\rho_m(L \mid z, \nu)\ d[\log_m(L)] \equiv \rho(L \mid z, \nu)\ dL$

$$\rho_m(L|z,\nu) = \ln(m) L \rho(L|z,\nu). \tag{15.13}$$

The weighted luminosity function, or "visibility function,"

$$\phi(L|z,\nu) \equiv L^{5/2}\rho(L|z,\nu) \tag{15.14}$$

introduced by von Hoerner (1973) emphasizes the contributions of sources in different luminosity ranges to the weighted source count $S^{5/2}\ n(S \mid \nu)$ (Section 15.4.2). In the low-redshift (static Euclidean) limit $L = 4\pi\ D^2\ S$ and $dV = 4\pi\ D^2\ dD$, the number $n(L, D \mid \nu)\ dL\ dD$ of sources per steradian with luminosities L to $L + dL$ and distances D to $D + dD$ is related to the local luminosity function by $n(L, D \mid \nu)\ dL\ dD = \rho(L \mid \nu)\ dL \times D^2\ dD$. The corresponding number $n(L, S \mid \nu)\ dL\ dS$ in the flux-density range S to $S + dS$ is given by $n(L, S \mid \nu) = n(L, D \mid \nu) |\ dD / DS|$. The total number $n(S \mid \nu)$ of sources per steradian with flux densities S to $S + dS$ is

$$n(S|\nu) = \int_0^\infty n(L,S|\nu)dL = \frac{1}{2(4\pi)^{3/2}S^{5/2}} \int_0^\infty L^{3/2}\rho(L|\nu)dL. \tag{15.15}$$

This can be rearranged to yield

$$S^{5/2}n(S|\nu) = \frac{\ln 10}{2(4\pi)^{3/2}} \int_{-\infty}^\infty \phi(L|\nu)d[\log(L)]. \tag{15.16}$$

The local weighted luminosity function $\phi(L \mid z = 0, \nu = 1.4\ \text{GHz})$ is plotted in Figure 15.3(b). With Equation (15.16) it shows that, in the low-redshift limit, most radio sources selected at $\nu = 1.4$ GHz have luminosities $L \approx 10^{24}$ to 10^{27} W Hz^{-1} and are found in elliptical galaxies. Spiral galaxies contribute only about 1% of the sources; and radio-selected spiral galaxies have luminosities $L \approx 10^{22}$ W Hz^{-1}, about an order of magnitude higher than the typical radio luminosity of an optically selected spiral galaxy.

15.4.2. Source Counts

Because of the wide range of flux density and source density involved, no individual radio telescope can provide complete data, even at a single frequency (Figure 15.4). Pencil-beam instruments, large steerable dishes, and phased arrays are typically used to survey large regions of the sky to obtain statistically significant counts for the stronger sources with relatively low surface densities. Separate surveys made from the northern and southern hemispheres are necessary to cover the whole sky, and all-sky catalogues at $\nu = 0.408$, 2.7, and 5 GHz have been complied from large-scale radio surveys (Robertson 1973, Wall and Peacock 1985, and Kuhr et al. 1981, respectively). A number of pencil-beam surveys go much deeper than the all-sky surveys over limited areas. Synthesis instruments provide the most sensitive surveys, but only in very small regions of the sky, typically 10^{-5} to 10^{-3} sr. Counts of very faint sources based on only a few such small fields may be subject to error if there is significant clustering. Nevertheless, in contrast to the early radio source surveys (cf. Jauncey 1975), modern data obtained by different observers using very different kinds of radio telescopes are in good agreement with respect to individual source positions and flux densities as well as surface densities.

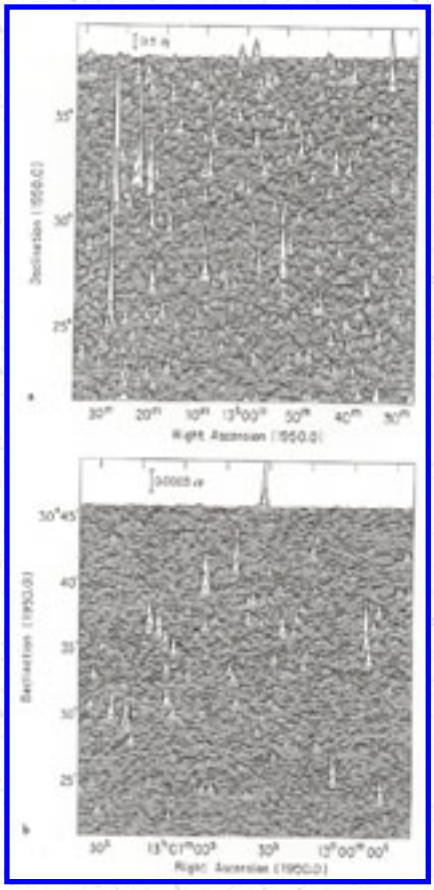

Figure 15.4. Profile plots of the sky near the north galactic pole mapped with (a) the NRAO 91-m telescope (beamwidth ≈ 12') (Condon and Broderick 1985) and (b) the VLA (beamwidth 17".5) (Mitchell and Condon 1985) illustrate the range of source intensities and sky densities that go into the ν = 1.4 GHz source count. (From Condon 1984.)

The number $n(S \mid \nu)\, dS$ of sources per steradian with flux densities S to $S + dS$ found in a survey made at frequency ν is called the *differential* source count; the total number per steradian stronger than S, $\int_S^\infty n(s \mid \nu)\, ds$, is called the *integral* source count. Integral counts are rarely used any more because they smear rapid changes of source density with flux density and the numbers are not statistically independent from one flux-density level to the next (Jauncey 1967, Crawford et al. 1970). The steep slopes of the differential source counts tend to obscure features in graphical presentations, so the counts are usually either weighted (simply multiplied by $S^{5/2}$) or normalized [divided by the count $n_0(S \mid \nu) = k_0 S^{-5/2}$ expected in a static Euclidean universe; the constant k_0 is usually set so that $n(S \mid \nu) / n_0(S \mid \nu) \approx 1$ at S = 1 Jy] before plotting. Historically, this normalization has been used to facilitate comparisons with the static Euclidean count - level portions of the actual normalized counts are said to have a "Euclidean slope," for example. Such comparisons can be misleading, however, because the static Euclidean

approximation has surprisingly little relevance to the actual source counts except at the very highest flux densities (cf. Section 15.9). In particular, a Euclidean slope does not signify that the sources in that flux-density range have low redshifts or are not evolving.

Source counts covering a wide range of flux densities are currently available at ν = 0.408, 0.61, 1.4, 2.7, and 5 GHz (cf. Condon 1984b). The most extensive is at ν = 1.4 GHz and is shown in Figure 15.5. The NRAO 91-m telescope was used to measure the flux densities of sources stronger than S = 2 Jy at ν = 1.4 GHz (Fomalont et al. 1974) and also in the $0.175 \leq S < 2$ Jy range (Machalski 1978). The fainter levels are based on VLA "snapshot" surveys (Condon et al. 1982b, Mitchell 1983; Coleman et al. 1985), the WSRT deep survey of the Lynx area (Oort 1987), and the deepest VLA survey (Mitchell and Condon 1985). The sky densities of sources too faint to be detected and counted individually in the latter survey were estimated statistically from their contribution to the map fluctuation or "P(D)" distribution (Scheuer 1957, 1974, Condon 1974) and are indicated by the shaded region extending down to S = 10 μJy. The integrated emission from extragalactic sources can be used to constrain the source count at even fainter levels. After subtracting galactic emission, Bridle (1967) obtained $T \approx 30$ K at ν = 178 MHz, corresponding to $T \approx 0.1$ K at ν = 1.4 GHz. The contribution $T(S) = [c^2 / (2k\,\nu^2)] \int_S^\infty sn(s)\,ds$ from sources stronger than S = 10 μJy is about 0.08 K, so the bulk of the extragalactic background can be accounted for by known source populations.

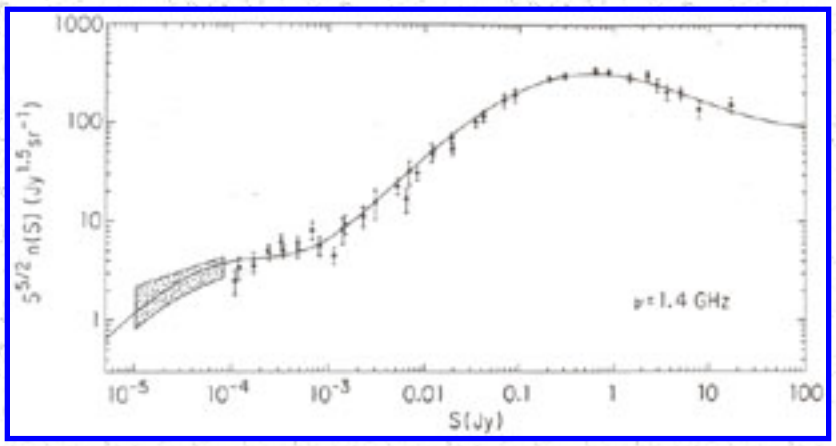

Figure 15.5. Weighted source count at ν = 1.4 GHz. Abscissa: flux density (Jy). Ordinate: weighted source count $S^{5/2}\,n(S)$ (Jy$^{1.5}$ sr^{-1}).

Most sources found in low-frequency surveys have power law spectra with spectral indices near $\alpha \approx +0.8$, but some have the more complex spectra and lower spectral indices ($\alpha \approx 0$) indicative of synchrotron self-absorption in compact ($\theta < 0.''01$) high-brightness ($T \approx 10^{11}$ K) components. These two source types are effectively distinguished by the simple criterion $\alpha \geq 0.5$ ("steep-spectrum" source) or $\alpha < 0.5$ ("flat-spectrum" source). The flat-spectrum sources can usually be identified with quasars, while most steep-spectrum sources are associated with galaxies (or empty fields if the galaxies are too distant). Many flat-spectrum sources vary in both intensity and structure on time scales of years, and their apparent luminosities may be affected by relativistic beaming (see Chapter 13). The evolutionary histories of these two source types may also differ. Being so compact, flat-spectrum sources are

probably less sensitive than extended steep-spectrum sources to changes in the average density of the intergalactic medium or in the energy density of the microwave background radiation with cosmological epoch (Rees and Setti 1968). Finally, flat-spectrum sources can be seen at greater redshifts because they are not so strongly attenuated by the $(1 + z)^{1+\alpha}$ Doppler term in Equation (15.1). For these reasons, it is worthwhile to separate the steep- and flat-spectrum sources and count them independently when possible. The numbers of flat-spectrum ($\alpha < 0.5$) and steep-spectrum ($\alpha \geq 0.5$) sources are comparable in high-frequency samples, and their counts at 5 GHz are plotted separately in Figure 15.6. The data were taken from Pauliny-Toth et al. (1973), Condon and Ledden (1981), Owen et al. (1983), and Fomalont et al. (1984).

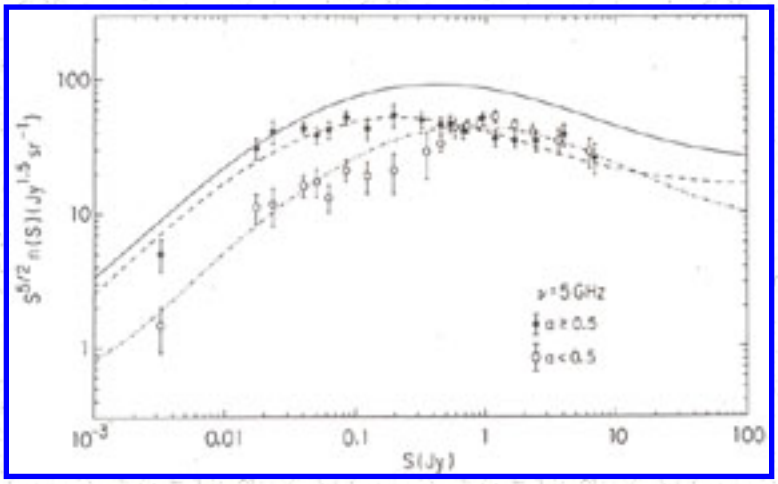

Figure 15.6. Weighted counts of steep-spectrum ($\alpha \geq 0.5$) (filled symbols) and flat-spectrum ($\alpha < 0.5$) (open symbols) sources found at $\nu = 5$ GHz, along with model predictions. (From Condon 1984b) (dashed and dot-dashed lines, respectively). Since the weighted counts of these two spectral populations are comparable but peak at slightly different flux densities, their sum (solid line) has a very broad peak.

15.4.3. Spectral-Index Distributions

Two-point spectral indices $\alpha(\nu_1, \nu_2)$ have been measured between $\nu_1 \approx 1.4$ GHz and $\nu_2 \approx 5$ GHz for a number of flux-limited source samples. The integral number $N(\alpha | S, \nu)\, d\alpha$ of sources per steradian with spectral indices α to $\alpha + d\alpha$ and flux densities $\geq S$ at frequency ν is shown for $S \geq 0.8$ Jy at $\nu = 5$ GHz in Figure 15.7(a). This (unnormalized) spectral-index distribution consists of a narrow steep-spectrum component with $\langle\alpha\rangle \approx 0.7$ and a broader flat-spectrum component centered on $\langle\alpha\rangle 0.0$. As the sample selection frequency ν is lowered, the number of steep-spectrum sources increases rapidly and the median spectral indices $\langle\alpha\rangle$ of both components increase. The increase in $\langle\alpha\rangle$ of each spectral component is proportional to the square of its width (Kellermann 1964), so the median spectral index of the flat-spectrum component changes more rapidly with frequency. These effects can be seen by comparing

Figure 15.7(a) with the spectral-index distribution of sources stronger than S = 2 Jy at ν = 1.4 GHz [Figure 15.7(b)]. The fraction of flat-spectrum sources may also change with the sample flux-density limit S at a given frequency ν. Figure 15.7(c) gives the spectral-index distribution of fainter ($S \geq 0.035$ Jy) sources selected at ν = 4.8 GHz.

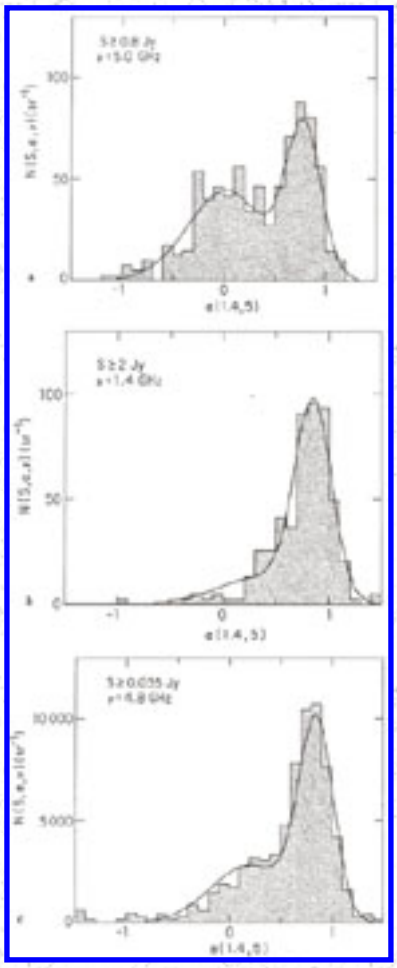

Figure 15.7. (a) Spectral-index distribution of 320 sources stranger than S = 0.8 Jy at ν = 5 GHz (Witzel et al. 1979). (b) Spectral-index distribution of 202 sources stronger than S = 2 Jy at ν = 1.4 GHz as compiled by Condon (1984b). (c) Spectral-index distribution of 479 sources stronger than S = 0.035 Jy at ν = 4.8 GHz (Owen et al. 1983). Abscissas: spectral index between 1.4 and 5 GHz. Ordinates: number of sources per steradian per unit α.

15.4.4. Redshift/Spectral-Index Diagrams

A plot of the integral number $N(\alpha, z \mid S, \nu)\, d\alpha\, d[\log(z)]$ of sources per steradian stronger than S at frequency ν with spectral indices α to $\alpha + d\alpha$ and redshifts $\log(z)$ to $\log(z) + d[\log(z)]$ shows the correlation of α on z (or L) for steep-spectrum sources (Laing and Peacock 1980, and references therein). Such a redshift/spectral-index diagram for sources with $S \geq 2$ Jy at $\nu = 1.4$ GHz is plotted in Figure 15.8.

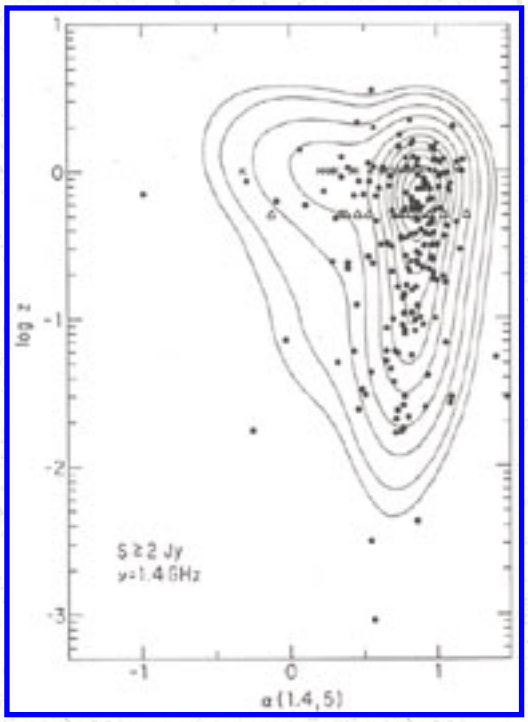

Figure 15.8. Redshift/spectral-index diagram for a sample of 202 sources in 3.86 sr stronger than $S = 2$ Jy at $\nu = 1.4$ GHz. Quasar candidates are indicated by crosses at $z \approx 1$, and empty fields by triangles at $z \approx 0.5$. Abscissa: spectral index between 1.4 and 5 GHz. Ordinate: log redshift. Contours: 1, 2, 5, 10, 20, 30, 40, 50, 60, and 70 sr^{-1}.

15.4.5. Redshift and Luminosity Distributions of Strong Sources

Spectroscopic redshifts exist for nearly all 3CR sources stronger than 10 Jy at 178 MHz (Laing et al. 1983, Spinrad et al. 1985) and for most of the stronger flat-spectrum sources found in high-frequency radio surveys (Kühr et al. 1981, Véron-Cetty and Véron 1983, Wall and Peacock 1985). Photometric redshifts of the remaining strong sources identified with galaxies can be estimated from Hubble relations such as $\log(z) \approx (m\nu - 22.5) / 6$ valid for first-ranked cluster galaxies and 3CR and 4C radio galaxies (van der Laan and Windhorst 1982, Windhorst 1986); empty-field sources can be treated as galaxies just fainter than the plate limit. Redshift distributions of quasar candidates may be approximated by the redshift distributions of known quasars or by a broad Hubble relation (Wall and Peacock 1985). Let $N(z \mid$

S, ν) d[log(z)] be the integral number of sources per steradian with redshifts log(z) to log(z) + d[log(z)] and stronger than S at frequency ν. Such an (unnormalized) redshift distribution of 202 extragalactic sources stronger than S = 2 Jy at ν = 1.4 GHz is shown in Figure 15.9.

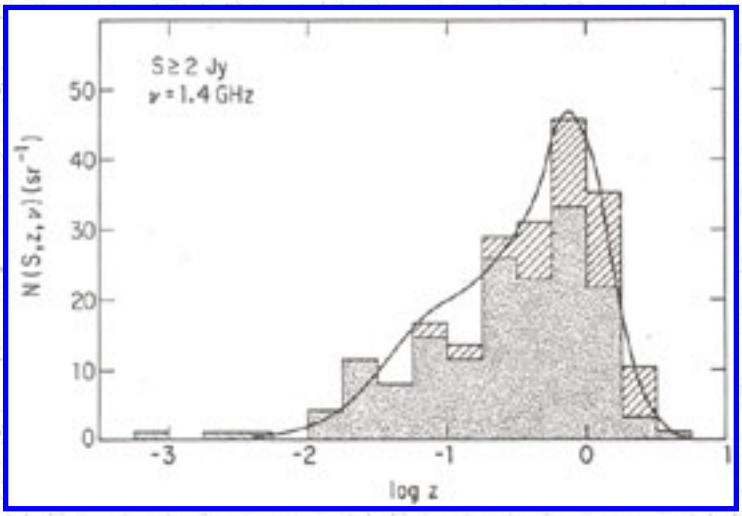

Figure 15.9. Redshift distribution of 202 sources stronger than S = 2 Jy at ν = 1.4 GHz. Spectroscopic redshifts are indicated by heavy shading, estimated redshifts by hatching. Abscissa: log redshift. Ordinate: number of sources per steradian per decade of redshift.

Since most of the sources in a flux-limited sample are within a factor of two of the flux-density limit, the integral luminosity distribution $N(L|\, S, \nu)\, d$[log(L)], or number of sources per steradian with luminosities log(L) to log(L) + d[log(L)] that are stronger than flux density S at frequency ν, can be used almost interchangeably with the integral redshift distribution. However, both of these distributions bin the (S, z)-data and hence do not make the most efficient possible use of the strong-source data (Peacock 1985).

15.4.6. Optical Constraints

The magnitude distributions of galaxies identified with faint radio sources are often used to estimate redshift distributions. These estimates can be refined if broadband colors and optical morphologies are available, since the absolute magnitudes of the giant elliptical galaxies associated with the most luminous radio sources are somewhat brighter than those of elliptical galaxies identified with less luminous sources (Auriemma et al. 1977) and the "blue" population of galaxies investigated by Kron et al. (1985). Windhorst et al. (1984a) have shown that the fraction of radio sources identified with galaxies brighter than $J \approx 23.7$ is about 50%, nearly independent of 1.4-GHz flux density in the range of 1 to 100 mJy. Thus, the median redshift in this flux-density range is roughly equal to the redshift of a giant elliptical galaxy at their plate limit, $z \approx 0.8$. Unless the amount of evolution changes discontinuously at redshifts just beyond $z \approx 0.8$, most of the remaining objects fainter than $J \approx 23.7$ must have redshifts only slightly larger. In fact, the identification rate approaches 100% at $V \approx 26$ (Windhorst 1986), and

few galaxies in this flux-density range should have redshifts greater than 1.9.

The identification content appears to change below $S \approx 1$ mJy from primarily red elliptical galaxies to bluer, morphologically distorted galaxies with fainter absolute magnitudes (Windhorst 1984, Kron et al. 1985). The nature of these galaxies and their redshift range is still uncertain (Wall et al. 1986, Windhorst 1986, Weistrop et al. 1987).

15.5. EVOLUTIONARY MODELS

The principal goals of evolutionary models are (1) to estimate the generalized luminosity function $\rho_m(L, \alpha,... | z, \nu)$ of radio sources, (2) to explain significant features in the observed source counts, spectral-index distributions, redshift distributions, etc. (e.g., Kellermann 1972), and (3) to identify new observations that will constrain future models most effectively. Existing data cannot fully determine the evolving luminosity function, so practical models incorporate additional *assumptions* about source evolution. The computations must be simplified by *approximations* as well - source spectra are taken to be simple power laws, spectral-index distributions may be replaced by Gaussians or even δ-functions, and evolution may be described by smooth functions with a limited number of free parameters.

A typical model-generating procedure is:

1. Choose a particular world model to fix the effective distance D and the volume element dV (Section 15.2). The Einstein-de Sitter ($\Omega = 1$) model is most commonly picked, but changing Ω has only a small, easily estimated effect (Peacock 1985).

2. Guess a form for the evolving luminosity function.

3. Compute the model local luminosity function, source counts, spectral index distributions, etc. and compare them with the data.

4. Revise the luminosity function.

5. Repeat steps (3) and (4) until satisfactory agreement is reached.

Differences between the models produced by different authors reflect their different data sets, assumptions about the type of evolution occurring, computational approximations, and methods for deciding that a model is satisfactory. Steps (2) and (4) are not straightforward, although simplified models (Section 15.9) can make the relations between the input luminosity function parameters and the output observables clearer.

15.5.1. Source Distribution Equations

The actual spectra of radio sources are normally approximated by power laws so that the spectral luminosity function at all frequencies ν is determined by the spectral luminosity function at any one frequency ν_0 from

$$\rho_m(L, \alpha|z, \nu) = \rho_m \left[\left(\frac{\nu}{\nu_0} \right)^{\alpha} L, \alpha|z, \nu_0 \right] \tag{15.17}$$

for a measured between *any* two frequencies. Models based on this approximation generally work well at ν = 408 MHz and higher frequencies, but they overestimate the 178-MHz source count significantly (Peacock and Gull 1981, Condon 1984b). Both 178-MHz flux-density scale errors and genuine spectral curvature caused by synchrotron self-absorption may contribute to this discrepancy.

The total number of sources with luminosities L to $L + dL$ spectral indices α to $\alpha + d\alpha$, at frequency ν, and lying in the spherical shell with comoving volume dV at redshift z is

$$\rho(L, \alpha|z, \nu) dL d\alpha dV. \tag{15.18}$$

The number of sources in this shell equals the total number $\eta(S, \alpha, z \mid \nu)\, dS\, d\alpha\, dz$ of sources with flux densities S to $S + dS$ spectral indices α to $\alpha + d\alpha$, and redshifts z to $z + dz$ found in a survey of the whole sky (4π sr) at frequency ν. Weighting by $S^{5/2}$ and eliminating both dV and dL / dS yields

$$S^{5/2} \eta(S, \alpha, z|\nu) = \frac{c \phi(L, \alpha|z, \nu) dz}{(4\pi)^{1/2} H_0 D (1 + \Omega z)^{1/2} (1 + z)^{5/2 + 3\alpha/2}}. \tag{15.19}$$

Integrating over redshift and dividing by 4π gives the weighted (spectral) source count $S^{5/2}\, n(S, \alpha \mid \nu)$, where $n(S, \alpha \mid \nu)\, dS\, d\alpha$ is the number of sources per steradian with flux densities S to $S + dS$ and spectral indices α to $\alpha + d\alpha$ found at frequency ν:

$$S^{5/2} n(S, \alpha|\nu) = \frac{c}{(4\pi)^{3/2} H_0} \int_0^{\infty} \frac{\phi(L, \alpha|z, \nu) dz}{D (1 + \Omega z)^{1/2} (1 + z)^{5/2 + 3\alpha/2}}. \tag{15.20}$$

The distribution equations (15.19) and (15.20) can be integrated numerically to give the observables described in Section 15.4. Using the weighted luminosity function ϕ to calculate the weighted source count directly minimizes the interpolation errors that can be significant in numerical integrations of the more rapidly varying luminosity function ρ_m (cf. Danese et al. 1983, Peacock 1985) to obtain the unweighted source count.

The weighted differential source count $S^{5/2}\, n(S \mid \nu)$ at frequency ν (Section 15.4.2) is

$$S^{5/2} n(S|\nu) = \int_{-\infty}^{\infty} S^{5/2} n(S, \alpha|\nu) d\alpha. \quad (15.21)$$

The (unnormalized) spectral-index distribution $N(\alpha \mid S, \nu)$ (Section 15.4.3) is obtained by integrating the differential spectral count:

$$N(\alpha|S, \nu) = \int_{S}^{\infty} n(s, \alpha|\nu) ds. \quad (15.22)$$

The redshift/spectral-index diagram (Section 15.4.4) shows the values of $N(\alpha, z \mid S, \nu)$ given by

$$N(\alpha, z|S, \nu) = \frac{\ln 10}{4\pi} \int_{S}^{\infty} z\eta(s, \alpha, z|\nu) ds. \quad (15.23)$$

The (unnormalized) integral redshift distribution $N(z| S, \nu)$ (Section 15.4.5) is found by integrating over α:

$$N(z|S, \nu) = \int_{-\infty}^{\infty} N(\alpha, z|S, \nu) d\alpha. \quad (15.24)$$

Most radio sources in any flux-limited sample have flux densities only slightly higher than the flux-density limit, so redshift and luminosity are strongly correlated. Thus the integral luminosity distribution $N(L| S, \nu)$ can be used instead of the integral redshift distribution $N(z| S, \nu)$. Let $n(L, S, \alpha \mid \nu)\, d[\log(L)]\, dS\, d\alpha$, be the differential number of sources per steradian with luminosities $\log(L)$ to $\log(L) + d[\log(L)]$, flux densities S to $S + dS$ and spectral indices α to $\alpha + d\alpha$ at frequency ν. Then, $4\pi n(L, S, \alpha \mid \nu)\, d[\log(L)] = \eta(S, \alpha, z \mid \nu)\, dz$ and

$$n(L, S, \alpha|\nu) = \frac{\ln(10)\eta(S, \alpha, z|\nu)}{4\pi} \left[\frac{L}{(dL/dz)}\right] \quad (15.25)$$

where

$$\left[\frac{L}{(dL/dz)}\right] = \left(\frac{1+\alpha}{1+z} + \frac{2}{D}\frac{dD}{dz}\right)^{-1} \quad (15.26)$$

and

$$\frac{2}{D}\frac{dD}{dz} = \frac{2\Omega[1+(\Omega/2-1)(\Omega z+1)^{-1/2}]}{\Omega z+(\Omega-2)[(1+\Omega z)^{1/2}-1]} - \frac{2}{1+z}. \quad (15.27)$$

Integrating Equation (15.25) over flux density and spectral index yields the (unnormalized) integral luminosity distribution

$$N(L|S,\nu) = \int_S^\infty \int_{-\infty}^\infty n(L,s,\alpha|\nu)\,d\alpha\,ds. \quad (15.28)$$

15.5.2. Evolutionary Models of Radio Luminosity Functions

Ryle and Clarke (1961) showed that their 178-MHz source count above S = 0.25 Jy is incompatible with nonevolving Einstein-de Sitter and steady-state models. They also recognized that "the introduction of evolutionary effects which appear to be necessary will make the selection of a unique [world] model difficult." In a paper introducing many of the features found in subsequent model calculations, Longair (1966) modeled the 178-MHz source count, strong-source luminosity distribution, and integrated emission from discrete sources in an evolving Einstein-de Sitter universe. "Power-law" evolution proportional to $(1 + z)^n$ yielded satisfactory fits only if restricted to the most luminous sources and truncated at high redshifts. "Exponential" evolution proportional to $e^{-t/\tau}$, where t is the cosmic time and τ the evolutionary time scale, was proposed by Rowan-Robinson (1970) because it does not diverge at high redshifts. Although this parametric form shows that the data do not require a real truncation of evolution at large z, Rowan-Robinson also considered *physical* factors that must ultimately truncate evolution, such as the time needed to form the parent galaxies of radio sources and electron energy losses by inverse Compton scattering off the microwave background radiation. A parametric model explicitly constrained by astrophysical assumptions was tried by Grueff and Vigotti (1977) to explain the 408-MHz source count and the luminosity distributions of sources stronger than S = 10 Jy and S = 0.9 Jy. They assumed that quasars form at z = 2.5 and evolve into galaxies whose radio-emitting lifetimes are inversely proportional to their radio luminosities. One difficulty with this model is that the evolution of low-luminosity radio sources can be minimized only if their radio emitting lifetimes are comparable with the Hubble time.

Extensions of the source counts to lower flux densities and the availability of more complete redshift data for strong sources eventually justified reexamination of the first parametric models. Wall et al. (1980) found that the 408-MHz source count extending to S = 0.01 Jy and the "all-sky" luminosity distribution of sources stronger than S = 10 Jy were sufficient to show that "power law" models are a poor representation of the cosmological evolution of powerful radio sources. They also investigated "exponential" evolution of the form $\exp[M(1 - t / t_0)]$, where M specifies the strength of the evolution and t_0 is the present age of the universe. Successful models were constructed in which M depends on luminosity [e.g., $M = 0$ for $L < L_1$, $M = M_{max}$ for $L > L_2$, and $M = M_{max}(\log L - \log L_1) / (\log L_2 - \log L_1)$ for $L_1 < L < L_2$] or redshift. Robertson's (1978, 1980) "free-form" analysis of essentially the same data

did not assume a functional form for the redshift dependence of evolution, but used the data to *solve* for it. However, these data cannot fully determine both the redshift and luminosity dependence of the evolution, so Robertson did assume a parametric form for the luminosity dependence that is similar to the one specified above. An artifact of the rather sharp changes of evolution with luminosity implied by this parametric form is a markedly bimodal redshift distribution at low flux densities (cf. Figure 10 of Wall et al. 1980).

The preceding models approximate the spectral-index distributions of all sources by a single δ-function centered on $\alpha \approx 0.8$, and they work well for data selected at any one low ($\nu < 1$ GHz) frequency. Extensive sky surveys made at 2.7 and 5 GHz in the late 1960s revealed significant populations of sources with $\alpha \approx 0$ and led to models accounting for both the steep- and flat-spectrum sources simultaneously (Schmidt 1972, Fanaroff and Longair 1973, Petrosian and Dickey 1973). The decline in the fraction of flat-spectrum sources as the 5-GHz sample flux-density limit is decreased below $S \approx 1$ Jy (Figure 15.6) can be reproduced if (1) the local spectral luminosity function is separated or "factorized" into independent spectral-index and luminosity functions at some frequency of lower than 5 GHz and (2) the rate of evolution is the same for both steep- and flat-spectrum sources. Then there is an inverse correlation induced between a and L at higher frequencies, and the weighted 5-GHz count of flat-spectrum sources peaks at a higher flux density than the weighted count of steep-spectrum sources.

There have been some indications that flat-spectrum quasars may evolve less than steep-spectrum or optically selected quasars. The weighted count of flat-spectrum sources (mostly quasars) peaks near $S \approx 1$ Jy (Figure 15.6), so the *average* count slope is nearly Euclidean for the flat-spectrum sources found in the first large-scale 5-GHz surveys that are complete down to $S \approx 0.6$ Jy. Because the source count slope and $\langle V / V_m \rangle$ (< ahref="Condon4.html#4.1">Section 15.4.1) are closely related (Longair and Scheuer 1970), quasar identifications of flat-spectrum sources from these surveys have nearly static-Euclidean values $\langle V / V_m \rangle \approx 0.5$ (Schmidt 1976), much lower than the $\langle V / V_m \rangle \approx 0.7$ of quasars identified with primarily steep-spectrum 3CR quasars stronger than $S = 9$ Jy at $\nu = 178$ MHz (Schmidt 1968). While high $\langle V / V_m \rangle$ values indicate evolution, $\langle V / V_m \rangle \approx 0.5$ does not exclude evolution because the *distribution* of $\langle V / V_m \rangle$ may still be nonuniform. Evolution increasing at low redshifts ($z < 2$, for example) and decreasing at higher redshifts still in the sample volumes V_m could yield a nonuniform V / V_m distribution with $\langle V / V_m \rangle \approx 0.5$. Just this situation is probably occurring. The 3CR quasars can be seen only out to limiting redshifts $z_m \approx 2$, and their large $\langle V / V_m \rangle$ value reflects monotonically increasing evolution up to $z \approx 2$; flat-spectrum quasars stronger than $S = 0.6$ Jy can be seen at higher redshifts ($z_m \approx 3$ or 4) where their evolution has started to decline. Kulkarni (1978) produced models that allow the steep- and flat-spectrum populations to evolve independently, approximate the spectral-index distributions of each population by Gaussians, and include the correlation of α with L among steep-spectrum sources. In both the Kulkarni (1978) and Machalski (1981) models, the flat- and steep-spectrum sources evolve differently, but later models by Peacock and Gull (1981) and Condon (1984b) show that these two spectral classes may indeed evolve at the same rates without violating the data constraints.

Condon (1984b) searched for a single model to fit *in detail* a wide range of available radio data (the local luminosity functions of spiral and elliptical galaxies at ν = 1.4 GHz; source counts at ν = 0.408, 0.61, 1.4, 2.7, and 5 GHz; counts of steep- and flat-spectrum sources at ν = 2.7 and 5 GHz; spectral-index distributions of sources in a number of samples complete to different flux-density limits at ν = 1.4, 2.7, and 5 GHz; redshift/spectral-index diagrams and redshift distributions of strong sources selected at 1.4, 2.7, and 5 GHz). The local 1:4-GHz visibility functions of spiral and elliptical galaxies were approximated by hyperbolas [< ahref="Condon4.html#Figure 3">Figure 15.3(b)]. The spectral luminosity function was "factorized" at ν_f = 1.4 GHz. The spectral-index function was approximated by two Gaussians, and the median spectral index of the steep-spectrum Gaussian varied with log(z). The evolution was constrained by the assumption that the *form* of the ν = 1.4 GHz luminosity function be independent of redshift:

$$\rho_m(L|z,\nu) = g(z)\rho_m[L/f(z)|z=0,\nu] \qquad (15.29)$$

where $f(z)$ and $g(z)$ are "free-form" functions that describe "luminosity evolution" and "density evolution," respectively. This "translation evolution" [so named because the evolution can be represented by translating the local luminosity function in the (log L, logρ_m)-plane] could result from evolutionary mechanisms that do *not* discriminate on the basis of source luminosity. A simple model was found that fits the radio data (curves in Figures 15.3, 15.5 - 15.9) as well as predicting redshift distributions (Figure 15.10) consistent with the magnitude distributions of faint-source identifications. Large values of the evolution function $E(L, z)$ (Figure 15.11) are restricted to high luminosities, as they must be to avoid producing too many faint sources. The luminosity range in which $E(L, z)$ is large is not a free parameter in this model; it is determined by the location of the bend near $L \approx 10^{25}$ W Hz^{-1} in the local luminosity function [Figure 15.3(a)]. Since this model assumes that all sources evolve equally, it demonstrates by example that restricting large $E(L, z)$ values to high luminosities does not imply that "only powerful sources evolve." Such an overinterpretation of the evolution function has led, for example, to the incorrect belief that only the (relatively luminous) radio quasars evolve, but that the (less luminous) radio galaxies do not.

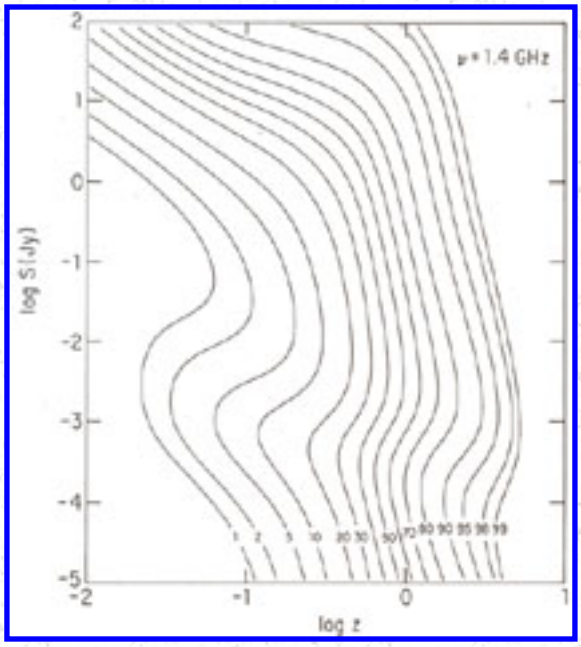

Figure 15.10. Model redshift distributions at ν = 1.4 GHz (From Condon 1984b). Abscissa: log redshift. Ordinate: log flux density (Jy). Parameter: percentage of sources at flux density S with redshifts less than z.

All of the models described above are based on strong assumptions about the form of evolution in the (L, z)-plane. They show that evolutionary forms consistent with the data exist, but these solutions are certainly not unique. In order to explore the *range* of luminosity functions consistent with the source counts at ν = 0.408, 2.7, and 5 GHz, luminosity distributions, and optical identification data, Peacock and Gull (1981) generated a number of "free-form" models in which the evolution is described by power series in log(L) and either log(1 + z) or log(1 - t / t_0) so that it is "free-form" in both luminosity and time, at least to the extent that evolution varies *smoothly* with these quantities. The possibility of a sharp cutoff at high z was also considered. Steep- and flat-spectrum sources were allowed to evolve independently, and their spectral-index distributions were approximated by δ-functions. This approximation affects theaccuracy with which the model can reproduce the radio data (Condon 1984b) but does not significantly increase the uncertainty of the derived evolving luminosity functions (Peacock 1985). Their successful models indicate that flat- and steep-spectrum sources evolve similarly, with only the most luminous sources exhibiting large changes in their comoving density with epoch. However, the density of sources in most areas of the (L, z)-plane is not well defined by the data. By locating the areas of greatest uncertainty, Peacock and Gull could specify the most important data still needed - source counts and redshift distributions of faint flat-spectrum sources in particular. The redshifts of forty-one flat-spectrum quasars with $S \geq 0.5$ Jy at ν = 2.7 GHz were later added to the Peacock and Gull (1981) data base, and they allowed Peacock (1985) to suggest that the density of powerful flat-spectrum sources *declines* between $z \approx 2$ and z 4 (unless the small number of quasars still lacking spectroscopic redshifts all have $z > 3$).

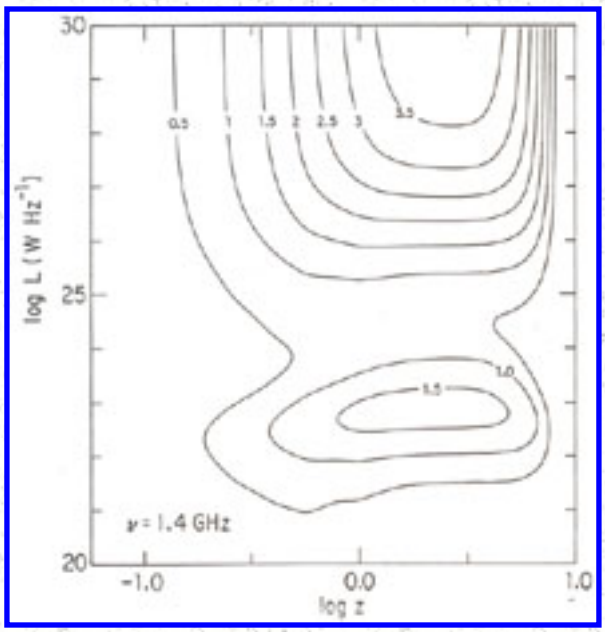

Figure 15.11. Contour plot of the Condon (1984b) model evolution function at ν = 1.4 GHz. Abscissa: log redshift. Ordinate: log luminosity (W Hz^{-1}). Contours: log evolution function.

15.6. SOURCE SIZE EVOLUTION

15.6.1. The Angular Size-Redshift Relation

Even though radio sources are not good "standard rods," some statistic describing their size distribution might be stable enough to permit direct measurements of size evolution in populations of optically identified radio sources with known redshifts.

Since the apparent size of a double radio source is always reduced by projection onto the sky, the maximum θ_m of the distribution of angular sizes θ will minimize projection errors. Miley (1971) plotted the angular sizes of strong radio galaxies (nearly all with $z < 0.3$) and quasars (nearly all with $z > 0.3$) versus redshift and found that their upper bound obeys the "static Euclidean" relation $\theta_m \propto 1 / z$. In any expanding Friedmann model, this result indicates either size evolution or an inverse correlation between luminosity and size for radio quasars.

These two effects can be distinguished by comparing radio quasars in a narrow luminosity range but widely separated in redshift; i.e., quasars found in surveys complete to different flux-density limits. Such a comparison of 3CR ($S \geq 10$ Jy at ν = 178 MHz) and 4C ($S \geq 2.5$ Jy at ν = 178 MHz) quasars (Hooley et al. 1978) was inconclusive because θ_m depends on small numbers of sources and hence is a fairly insensitive statistic. No size evolution was needed to fit the data, but size evolution of the form $d = d_0(1 + z)^{-N}$ with $N < 1.5$ could not be excluded.

A recent comparison of the median angular sizes $\langle\theta\rangle$ of radio galaxies with luminosities near $L \approx 10^{26}$ W Hz^{-1} found in three 1.4-GHz samples complete to S = 2, 0.55, and 0.01 Jy indicates size evolution in the range $1 < N < 2$ (Kapahi 1985). Although the formal statistical significance of this result is high, there remain two possible selection effects. (1) Only the faint-source sample was obtained from an aperture-synthesis survey that discriminates against sources larger than $\theta \approx 12''$. (2) Flux-limited surveys conducted at the same frequency ν but covering different redshift ranges are effectively complete at different emitted frequencies $\nu(1 + z)$. A correlation between linear size and either spectral index or frequency in the source frame will mimic size evolution. This angular size-redshift relation for median angular sizes has recently been extended to include quasars (Kapahi 1986), as shown in Figure 15.12.

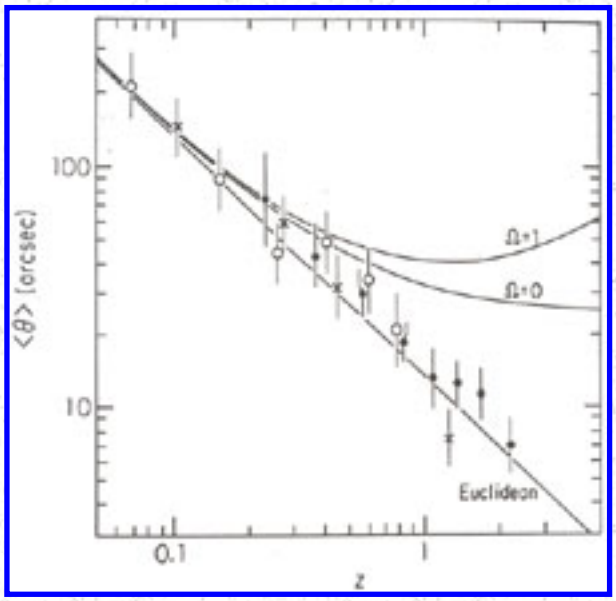

Figure 15.12. Median angular sizes of samples of galaxies (open circles), galaxies in a narrow luminosity range (crosses), and quasars (filled circles) (Kapahi 1986). The relation $\langle\theta\rangle \propto 1/z$ suggests size evolution in Friedmann models. Abscissa: redshift. Ordinate: median largest angular size (arcsec).

15.6.2. The Angular Size-Flux Density Data

Most steep-spectrum extragalactic sources can be resolved with sensitive aperture-synthesis telescopes, and their angular sizes θ are often by-products of deep surveys. Thus, fairly unbiased statistics describing the angular-size distributions of radio sources as a function of flux density can easily be obtained and used to estimate the linear size evolution of extragalactic sources. Unfortunately, the angular sizes of radio sources with differing morphologies are not easy to define precisely, the θ - S relation is rather insensitive to size evolution, and size evolution is either weak or nonexistent.

Radio sources at cosmological distances have angular sizes ranging from < 0."001 for the most compact flat-spectrum sources to several minutes of arc, so no one instrument can detect and resolve all of them. However, the majority of steep-spectrum sources stronger than $S \approx 1$ mJy are larger than $\theta \approx 10$ arcsec, making the *median* $\langle\theta\rangle$ of their broad angular-size distribution accessible to the aperture-synthesis telescopes used to make deep radio surveys.

A suitable *definition* of θ is complicated by the variety of source structures encountered. Ideally, θ should be a metric diameter, which is more sensitive to redshift and differences between world models than the isophotal diameters used in optical astronomy (Sandage 1961). A good working definition of θ should be insensitive to details of the source brightness distribution and observational limitations, low dynamic range and limited resolution especially. The traditional definition of θ is the component separation of a double source because most strong sources selected in low-frequency surveys have this morphology and also because their component separations are easy to measure directly from contour maps. Unfortunately, the measured value of θ depends on the component intensity ratio if the double source is barely resolved or observed with low dynamic range, and this definition must be generalized to the "largest angular size" before it can be applied to sources with core jet or more complex radio morphologies. However, the largest angular size is generally larger on maps of strong sources and can lead to an apparent change of θ with S. For example, the strong low-redshift quasar 3C273 is listed as having an angular size $\theta = 21$ arcsec (Kapahi et al. 1987) because its jet was mapped with high dynamic range. If 3C273 were moved to a high redshift and discovered as a faint source in an aperture-synthesis survey, its jet would not be distinguishable from the bright compact core, and its quoted angular size would be very small. Since the angular variances of the observing beam and the source brightness distribution $B(\phi)$ add under convolution, the angular diameter defined by $\theta^* \equiv 2[\int \phi^2 B(\phi)\, d\phi / \int B(\phi)\, d\phi]^{1/2}$ can be measured even for sources just large enough to broaden the beam (cf. Coleman 1985). It can be applied to any source morphology and it is independent of map dynamic range, except at very low signal-to-noise ratios where it may be overestimated by Gaussian fitting. Its main drawback is that it is more difficult to determine from contour plots.

Even with a good definition of θ, there are biases that affect the angular-size distribution of faint sources found in aperture-synthesis surveys. The survey maps are complete only above some *peak* flux density, so weak sources significantly larger than the synthesized beam (typically 10" to 20" FWHM) will be missed and must be corrected for. The sky density of sources fainter than a few mJy is so high that distinguishing physically associated components of double sources from unrelated projected pairs of compact sources becomes a problem (Condon et al. 1982b).

15.6.3. Models of the Angular Size-Flux Density Relation

All evolutionary models of the observed $\langle\theta\rangle$ - S relation (e.g., Figure 15.13) require as an input one of the models for the evolving radio luminosity function described in Section 15.5. Some estimate of the linear size distribution of sources covering a wide luminosity range (e.g., Figure 15.14) is also needed. The first detailed model (Kapahi 1975) was based on a luminosity function similar to that derived by Longair (1966). The approximation was made that the projected linear size d of a radio source is

independent of its luminosity L, and a parametric "local" size distribution was obtained by a fit to the size distribution of low-redshift ($z < 0.3$) 3CR sources. Power law size evolution in which source sizes vary as $d = d_0(1 + z)^{-N}$ was tried, and the value $N \approx 1.5$ gave the best fit to the $\langle\theta\rangle$ - S data for sources stronger than $S \approx 1$ Jy at 178 MHz.

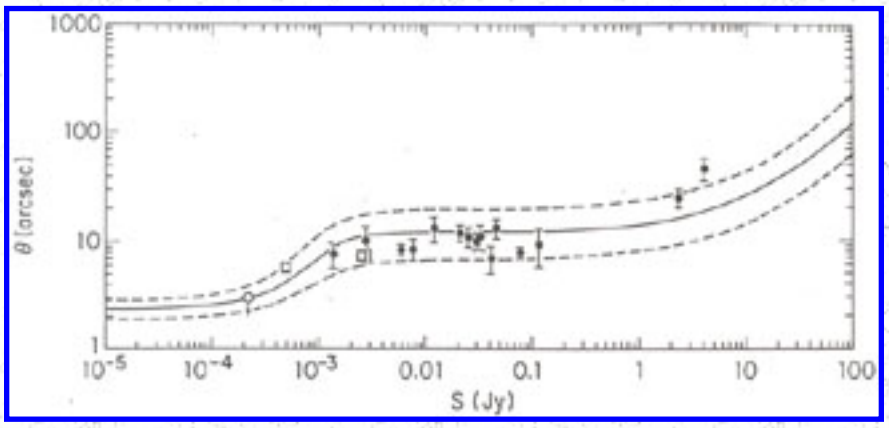

Figure 15.13. Median angular size as a function of 1.4-GHz flux density. The filled circles are from the compilation by Windhorst et al. (1984); the open circles and the upper limit are from the Coleman and Condon (1985) high-resolution VLA survey. The solid line is the median angular size from the Coleman and Condon (1985) model ($\Omega = 1$, no size evolution), while the dashed lines mark the 60th- and 40th-percentile angular sizes. Abscissa: flux density (Jy). Ordinate: median angular size (arcsec).

The $\langle\theta\rangle$ - S relation was extended to $S \approx 0.1$ Jy at 408 MHz by Downes et al. (1981). Their analysis was based on the improved Wall et al. (1980) radio luminosity functions. Instead of deriving a size distribution function, they assumed that individual 3CR sources are representative of the overall population of sources dominating the relevant epoch. Sources in their 3CR "parent population" were assigned weights by the weighted $1 / V'_m$, method used to calculate the local luminosity function of an evolving population (Section 15.4.1). This method should automatically account for any possible correlation between linear size and luminosity in the parent sample, but spreading the parent population over a number of luminosity bins increases the statistical uncertainties in each. Also, the 3CR parent population does not correct for possible morphological differences between the 3CR sources and sources appearing elsewhere in the (L, z)-plane. If there is a substantial population of steep-spectrum compact sources (compact sources with steep spectra at high frequencies but relatively flat spectra at lower frequencies) among the faint ($S < 0.1$ Jy) high-redshift sources found at 408 MHz, it will be better represented in a (lower-redshift) parent population selected at some frequency *higher* than 408 MHz (e. g., Fielden et al. 1983, Allington-Smith 1984). Although Downes et al. (1981) found no value of the evolution exponent N reproduced the data with the 3CR parent sample, Kapahi and Subrahmanya (1982) used the same methods and data to find acceptable fits in the range $1 < N < 1.5$. Kapahi et al. (1987)

attribute this discrepancy to a computational oversight by Downes et al. (1981). Using a parent sample selected at ν = 2.7 GHz with the Peacock and Gull (1981) multi-frequency luminosity functions to predict the $\langle\theta\rangle$ - S relation at other frequencies, Fielden et al. (1983) and Allington-Smith (1984) obtained good fits in the range 0.05 to 1 Jy at 408 MHz for $1 < N < 1.5$, but the stronger sources could not be accommodated simultaneously. Finally, Kapahi et al. (1987) modeled the $\langle\theta\rangle$ - S relation above $S \approx 0.1$ Jy at 408 MHz using a variety of luminosity functions and parent populations selected at 178, 1400, and 2700 MHz. They concluded that size evolution is always required.

Most faint ($S < 1$ Jy at ν = 1.4 GHz) sources probably have redshifts in the range $0.3 < z < 3$ for which the angular-size distance D_θ is nearly constant if $\Omega = 1$ (Figure 15.15). Without size evolution, changes in angular size with flux density reflect changes in linear size, not redshift. Flux density correlates more strongly with luminosity than with redshift for $S < 1$ Jy, so the flat portion of the $\langle\theta\rangle$ - S curve (Figure 15.13) can easily be matched without evolution if there is no correlation of linear size with luminosity (Figure 15.14). Conversely, models requiring evolution to fit this flat region generally have parent populations in which low-luminosity sources have larger median linear sizes than high-luminosity sources. The rather sharp drop in $\langle\theta\rangle$ below $S \approx 1$ mJy at ν = 1.4 GHz can be explained only by a correspondingly sharp drop in the median linear size of sub-mJy sources (Coleman and Condon 1985). This occurs naturally if the faintest sources are confined to the disks of spiral galaxies.

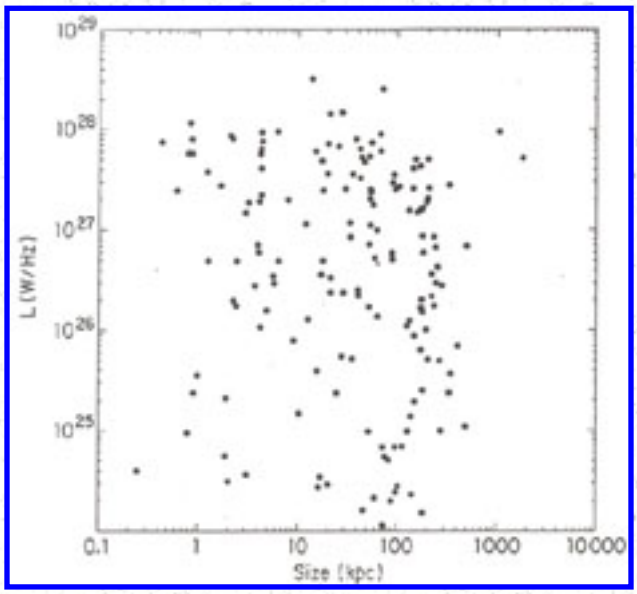

Figure 15.14. Projected linear size distribution of sources stronger than S = 2 Jy at ν = 1.4 GHz (From Coleman and Condon 1985) calculated for $\Omega = 1$. The correlation of size with luminosity is weak at best. Abscissa: projected linear size (kpc). Ordinate: 1.4-GHz luminosity (W Hz^{-1}).

All of the models above have trouble matching the rather steep rise of $\langle\theta\rangle$ at high flux densities. This

difficulty may be caused by the variation of θ with the dynamic range of the measurements. Using θ^* instead of θ for all sources reduces the rise above $S \approx 1$ Jy to the point that it can be fit without size evolution (Coleman 1985), although size evolution with $N \approx 1$ is still quite acceptable - the $\langle\theta\rangle$ - S relation is just not very sensitive to size evolution.

15.7. THE FAINT-SOURCE POPULATION

Recent VLA and WSRT deep surveys (Mitchell and Condon 1985, Oort 1987) have extended the 1.4-GHz source count to $S \approx 100\ \mu$Jy directly and $S \approx 10\mu$Jy statistically (Figure 15.5). The weighted source count flattens below $S \approx 1$ mJy, suggesting the emergence of a significant low-luminosity source population - $L < 10^{24}$ W Hz^{-1}) at $z \approx 1$, $L < 10^{22}$ W Hz^{-1} at $z \approx 0.1$. This luminosity range brackets the transition between elliptical and spiral galaxies in the local radio luminosity function (Figure 15.3), so the faint ($S < 1$ mJy) sources are likely to be quite different from the strong ones.

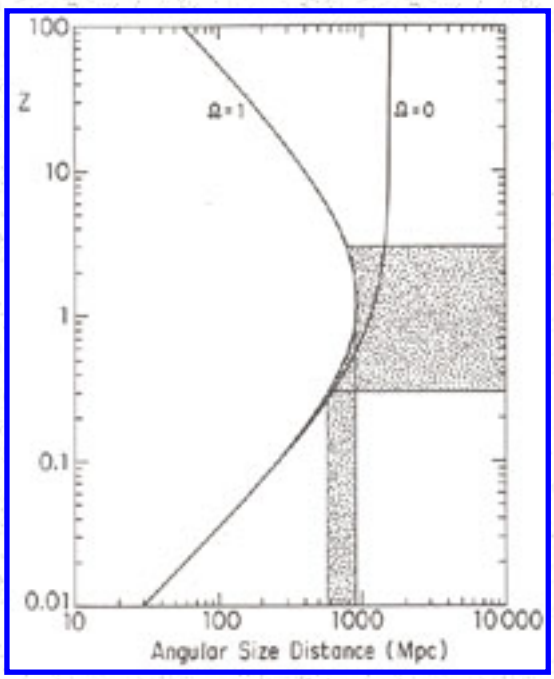

Figure 15.15. Most faint ($S < 1$ Jy at ν = 1.4 GHz) radio sources fall in the shaded redshift band $0.3 < z < 3$, so they are at nearly the same angular-size distance $D\theta$ if $\Omega = 1$. Abscissa: angular-size distance (Mpc). Ordinate: redshift.

Subrahmanya and Kapahi (1983) associated the faint sources with *nonevolving* spiral galaxies at low redshifts ($z < 0.1$). Their conclusion depends on a very steep local luminosity function (to yield a flat visibility function ϕ for $L < 10^{22}$ W Hz^{-1} derived from Pfleiderer's (1977) 1.4-GHz survey of bright spiral and irregular galaxies. Such a luminosity function implies much higher space densities of radio sources with $L < 10^{22}$ W Hz^{-1} than the luminosity function based on recent VLA observations of a

similar optical galaxy sample (Figure 15.3), probably because confusion by background sources in the larger beam of the NRAO 91-m telescope produces some spurious detections. The 1.4-GHz source count from nonevolving spiral galaxies described by the newer local luminosity function is an order of magnitude lower than the observed count, as indicated by the dotted line in Figure 15.17. With either luminosity function, the median redshift of nonevolving spiral galaxies in the flux-density range 0.1 to 1 mJy is only $\langle z \rangle 0.1$. Such a low median redshift does not appear to be consistent with the magnitude distribution of galaxies identified with faint sources selected at 1.4 GHz (Windhorst 1986).

If radio sources in spiral galaxies *do evolve* at about the same rate as those in elliptical galaxies (Condon 1984a, b), they can account for the flattening of the source counts below $S \approx 1$ mJy (Figure 15.5) as well as the higher redshifts (Figure 15.10) indicated by the optical-identification magnitude distribution. It should be emphasized that in this scenario, most of the faint radio sources are *not* the "normal" spiral galaxies found in optically selected catalogues. Typical radio-selected spiral galaxies are those with $L \approx 10^{22}$ W Hz^{-1} found at the peak of the visibility function, most of which are interacting "starburst" galaxies (e.g., Condon et al. 1982a), Markarian galaxies, and Seyfert galaxies (e.g., Meurs and Wilson 1984). Since there is a close correlation between the far-infrared ($\lambda = 60$ μm) and radio continuum flux densities of spiral galaxies, radio-selected spiral galaxies are more akin to galaxies found in the IRAS survey than to normal spiral galaxies.

A third explanation for the source-count flattening is that there is a "new population" of radio galaxies with $L \approx 10^{23}$ W Hz^{-1} at $\nu = 1.4$ GHz (Windhorst 1984) that was somehow missed by the radio luminosity functions derived from optically selected samples of spiral and elliptical galaxies (e.g., Figure 15.3) or Markarian and Seyfert galaxies (Meurs and Wilson 1984). Using spectroscopy and four-band photographic photometry of galaxies identified with radio sources stronger than $S = 0.6$ mJy (Kron et al. 1985), Windhorst (1984) estimated that the local space density of radio sources associated with his "blue galaxy" identifications exceeds that of radio sources in known spiral and elliptical galaxies by an order of magnitude in the luminosity range $L \approx 10^{22}$ to 10^{23} W Hz^{-1}. Only a moderate amount of evolution is needed for such a population to account for the source counts below $S \approx 5$ mJy (Windhorst et al. 1985).

The morphological composition of the blue radio-galaxy population is still unclear, and it may vary with both flux density and apparent magnitude. Those galaxies brighter than $F \approx 16$ mag are spiral galaxies; the fainter identifications "are often of peculiar compact morphology, sometimes interacting or merging" and have optical luminosities about equal to those of bright spiral galaxies (Windhorst 1984, Kron et al. 1985). Some of the faintest may be blue broad-line radio galaxies similar to those found in strong-source samples (Wall et al. 1986), photometrically misclassified elliptical galaxies (Kron et al. 1985), or misidentifications (Wall et al. 1986, Windhorst 1986, Weistrop et al. 1987). While the blue galaxies gradually displace red elliptical galaxies as the dominant population in faint radio-selected samples, it is not clear that they are a new population in the sense of surpassing the known local radio luminosity function near $L \approx 10^{23}$ W Hz^{-1}. If a weakly evolving population is significant in radio flux-limited samples at cosmological distances, it probably should be significant even in the small samples of optically bright galaxies used to construct the local luminosity function. Also, the radio identifications of

the large ($N \approx 10^4$) UGC galaxy sample (Nilson 1973) south of $\delta = +82°$ with sources stronger than S = 150 mJy at ν = 1.4 GHz (Broderick and Condon, manuscript in preparation) do not appear to be consistent with a factor-of-ten increase in the local luminosity function near $L = 10^{23}$ W Hz^{-1}. The UGC galaxies actually detected in this luminosity range are classified by Nilson as a mixture of active spirals, elliptical, S0, and "compact" galaxies. If the radio sources in this mixture evolve, they may account for most of the blue radio galaxies seen at cosmological distances in deep surveys. Because there is such a sharp decline in the luminosity function of spiral galaxies above $L \approx 10^{23}$ W Hz^{-1} the blue galaxy population identified with sources in the 1 to 10 mJy range by Kron et al. (1985) probably contains a smaller fraction of spiral galaxies than sub-mJy samples do.

A sharp distinction between radio-emitting spiral and elliptical galaxies can be made by the relative strengths of their far-infrared emission - nearly all infrared-selected galaxies with detectable radio sources are spirals, not ellipticals. Furthermore, there is a remarkably tight correlation between the far-infrared and radio continuum flux densities of spiral galaxies. For *infrared-selected* spirals, the quantity $u \equiv \log(S_{60\ \mu m} / S_{1.4GHz})$ has a median value $\langle u \rangle = +2.15 \pm 0.15$ and a scatter $\sigma_u < 0.3$ (Condon and Broderick 1986). Biermann et al. (1985) used the infrared-radio correlation and a static Euclidean extrapolation of the λ = 60 μm source count to predict that spiral galaxies will contribute significantly to the 5-GHz source count below $S \approx 100$ μJy. Now that the λ = 60 μn source count has been extended to S = 50 mJy (Hacking et al. 1987), the contribution of *infrared-selected* spiral galaxies to the 1.4-GHz count of sources as faint as S = 50 mJy / dex(u) = 0.35 mJy can be estimated directly from the infrared data - the weighted count scales as $u^{-3/2}$, so $S^{5/2}\, n(S \mid \nu = 1.4\ \text{GHz}) \approx 1$. At least 20% of the radio sources with $S \approx 0.35$ mJy at ν = 1.4 GHz can be identified with spiral galaxies in this way; if $\sigma_u > 0$, the percentage rises. Finally, the λ = 60 μn source count is consistent with strong evolution of infrared-selected spiral galaxies (Hacking et al. 1987).

15.8. ISOTROPY AND HOMOGENEITY

Radio sky maps should be very sensitive to fluctuations in the sky density of sources for the reasons given in Section 15.1. Radio sources appear to cluster about galaxies at least as much as galaxies cluster with galaxies (Longair and Seldner 1979), so radio source clustering in space should reflect large-scale inhomogeneities in the distribution of galaxies in space. However, the faint radio sources in any area of sky are spread along a line of sight almost $cz / H_0 \approx 3000$ Mpc in length, reducing the angular sensitivity to clustering in space by averaging over many clusters in the line of sight. Consequently, existing radio surveys are sensitive only to clustering on very large scales ($d > 100$ Mpc) at cosmological redshifts ($z \approx 1$), in contrast to optical (Bahcall and Burgett 1986, de Lapparent et al. 1986) and far-infrared (Meiksin and Davis 1986, Rowan-Robinson et al. 1986) surveys that probe nearby ($z \approx 0$) clustering on scales up to $d \approx 100$ Mpc.

Several different techniques have been used to search for fluctuations in the sky densities of radio sources. One is plotting the distribution of angular distances to the nearest neighbors of all sources in a survey and comparing this distribution with the expected random distribution (Maslowski et al. 1973).

The nearest-neighbor test is sensitive to clustering only in the small range of angular scales between the survey resolution and the typical separation between sources. Another simple procedure is to group the sources by position on the sky, flux-density range, etc. and compare their numbers with the expected Poisson distributions (Machalski 1977). A variation of this test for confusion-limited surveys is to divide the mapped region into small areas and compare the widths W of the $P(D)$ distributions in each (Hughes and Longair 1967). Then the effective number of sources sampled equals the number of beam areas in the whole map, potentially quite a large number. The distribution of widths W from the 480 squares, each covering $2° \times 2° \approx 91$ independent beam areas, from the Green Bank 1.4-GHz sky map overlapping the north galactic pole (Condon and Broderick 1985) is shown as a histogram in Figure 15.16. It is indistinguishable from the distribution expected in the absence of clustering (filled circles). Such grouping tests are most sensitive to clustering on the grouping scale chosen, so they must be repeated on a variety of scales. But they can easily be applied to surveys with irregular boundaries. More powerful tests for clustering of discrete sources are power spectrum analysis (Webster 1976a, b) based on the Fourier transform of a map with the sources replaced by δ-functions, and its Fourier-transform relative, correlation function analysis (Masson 1979). A significant advantage of correlation function analysis is that confusion anticorrelation affects only the smallest correlation lags but essentially all Fourier components of the fluctuation power spectrum.

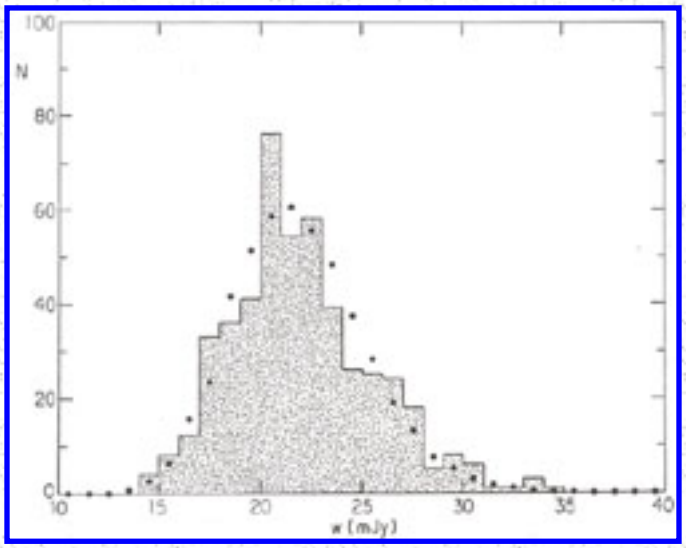

Figure 15.16. The observed widths W of the $P(D)$ distributions in 480 $2° \times 2°$ squares (histogram) and the expected width distribution (filled circles) if sources are not clustered. Abscissa: width (mJy). Ordinate: number of maps.

No convincing detection of anisotropy in the sky distribution of extragalactic radio sources has been made. The upper limits obtained are strong enough to rule out the "local hole" interpretation of the drop in the weighted source counts at high flux densities, but they do not yet strongly constrain clustering on scales $d < 100$ Mpc. This limitation is primarily statistical - the source density is too low in large-scale surveys. There are (very approximately) $N \approx [cz / (H_0\, d\,)]^3\, \omega / 3$ clusters of comoving size d in the cone

of solid angle ω. Only if the number n of sources in this solid angle is much greater than N can the statistical fluctuations be smaller than those caused by clustering. For $P(D)$ analysis of confusion-limited surveys, $n \approx \omega / \omega_b$, where ω_b is the beam area; and clustering on scales $d >> (\omega_b / 3)^{1/3}(c\ z / H_0)$ might be seen. The Green Bank 1.4-GHz sky map (Condon and Broderick 1985) has $\omega_b \approx 10^{-5}$ sr and so reaches $d >> 50$ Mpc. Confusion-limited surveys with only moderately higher resolution may detect clustering on scales already known to exist in optical and infrared samples.

Finally, it should be noted that the speed v of the Earth relative to the extragalactic source frame produces a dipole anisotropy of amplitude $[2 + (\gamma - 1)(1 + \alpha)] / (v / c)$ in the differential count $n(S) \propto S^{-\gamma}$ of sources with spectral index α (Ellis and Baldwin 1984). This effect is just below current limits of detectability, requiring surveys covering $N \approx 2 \times 10^5$ beam areas with high gain accuracy.

15.9. COSMOLOGY MADE SIMPLE: THE SHELL MODEL

The evolutionary models described in Section 15.5 are based on complex numerical calculations that tend to obscure connections between important features in the data and the calculated radio luminosity functions, redshift distributions, etc. In contrast, von Hoerner (1973) demonstrated with analytic approximations the importance of the broad visibility function ϕ (Equation 15.14) to the radio Hubble relation and to the form of the source count. In a uniformly filled, static Euclidean universe, the visibility function has no effect on the form of the source count (Equation 15.16) or the Hubble relation. The visibility function is important only if its width, $\Delta \log L$, is greater than twice the redshift range, $\Delta \log z$, containing most radio sources. Thus, the actual distribution of extragalactic radio sources in distance (lookback time) is so nonuniform that features in the source counts should not be interpreted as perturbations from a static Euclidean count. A much better starting model for the radio universe is actually a hollow shell centered on the observer! This "shell model" reproduces many features of the data almost as well as the more elaborate models and clearly shows how they are related to the distribution of sources in space.

For sources with average spectral index $\langle\alpha\rangle$ the relation

$$S^{5/2} n(S|\nu) \approx \frac{1}{(4\pi)^{3/2}} \int_0^\infty \phi(L|z,\nu)(1+z)^{-9/4-3\langle\alpha\rangle/2} \frac{dz}{z} \qquad (15.30)$$

is a good approximation to the exact Equations (15.20) and (15.21) for all $0 \leq \Omega \leq 2$, $z < 5$ (Condon 1984a). If most radio sources are confined to a thin shell of thickness Δz_s at redshift z_s,

$$S^{5/2} n(S|\nu) \approx \frac{\phi(L|z_s,\nu)}{(4\pi)^{3/2}} (1+z_s)^{-9/4-3\langle\alpha\rangle/2} \left(\frac{\Delta z_s}{z_s}\right). \qquad (15.31)$$

We assume translation evolution so $\rho_m(L|\ z,\ \nu) = g(z)\ \rho_m[L / f\ (z)|\ z = 0,\ \nu]$. Let $g_s \equiv g(z_s)$ be the amount

of density evolution and $f_s \equiv f(z_s)$ be the amount of luminosity evolution at the shell redshift. Then, $\log[\phi(L \mid z_s, \nu)] = \log[\phi(L / f_s \mid z = O, \nu)] + 3\log(f_s)/2 + \log(g_s)$ and

$$\log[S^{5/2} n(S|\nu)] \approx -\frac{3}{2}\log(4\pi) + \log\left[\phi\left(\frac{L}{f_s}\middle| z=0,\nu\right)\right] + \frac{3}{2}\log(f_s) + \log(g_s) + \log\left(\frac{\Delta z_s}{z_s}\right) - \left(\frac{9}{4} + \frac{3}{2}\langle\alpha\rangle\right)\log(1+z_s). \quad (15.32)$$

The redshift distribution of sources stronger than $S = 2$ at $\nu = 1.4$ GHz (Figure 15.9) suggests $z_s \approx 0.8$ and $(\Delta z_s / z_s) \approx 1$; the spectral-index distribution [Figure 15.7(b)] gives $\langle\alpha\rangle \approx 0.7$. Substituting these quantities yields the following expression relating the weighted source counts, the local visibility function, and the evolution parameters at the shell redshift:

$$\log[S^{5/2} n(S|\nu)] \approx \log\left[\phi\left(\frac{L}{f_s}\middle| z=0,\nu\right)\right] + \frac{3}{2}\log(f_s) + \log(g_s) - 2.49. \quad (15.33)$$

The values of f_s and g_s that satisfy Equation (15.33) can be found graphically by superimposing the observed source counts and local visibility functions, as shown in Figure 15.17. For sources with $z_m \approx 0.8$ and $\alpha \approx 0.7$, $\log[L(\text{W Hz}^{-1})] - \log[S(\text{Jy})] \approx 26.9$. Since the best fit of the local visibility function to the source counts occurs at $\log[L(\text{W Hz}^{-1})] - \log[S(\text{Jy})] \approx 25.7$ (Figure 15.17), we require luminosity evolution in the amount $\log(f_s) \approx 26.9 - 25.7 = 1.2$. This fit also implies $\log[S^{5/2}\, n(S \mid \nu = 1.4\text{ GHz})] \approx \log[\phi(L \mid z = 0, \nu = 1.4\text{ GHz})] - 0.65$, resulting in $\log(g_s) \approx 0.0$ (no density evolution). With these evolution parameters, the weighted source count predicted by the shell model corresponds exactly to the local visibility function plotted as the solid line in Figure 15.17. The model actually reproduces the entire observed source count from $S \approx 10\mu$Jy to $S \approx 10$ Ky.

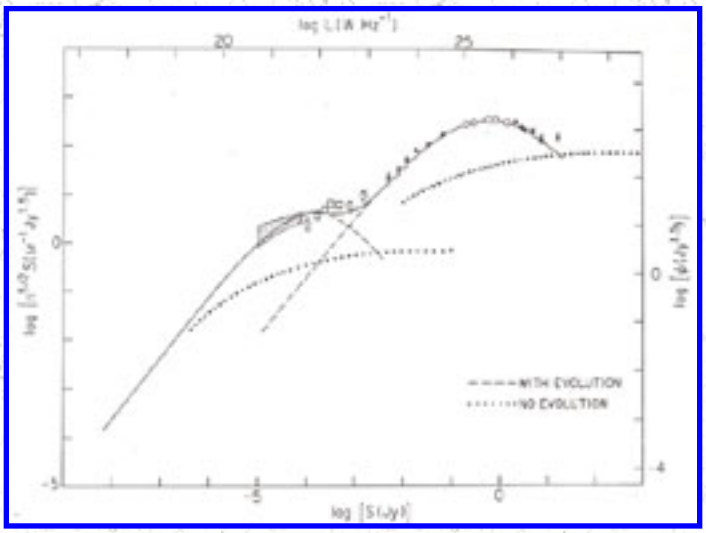

Figure 15.17. Superposition of the weighted source count at 1.4 GHz (data points) and the hyperbolic fits to the 1.4-GHz local visibility functions for radio sources in spiral and elliptical galaxies (dashed lines). The combined local visibility function for all radio sources is indicated by the solid curve. This curve also plots the weighted source count predicted by the shell model. The source counts expected from *nonevolving* populations of spiral and elliptical galaxies described by this local luminosity function are shown as dotted curves. Lower abscissa: log flux density (Jy). Left ordinate: log weighted source counts (sr^{-1} ($Jy^{1.5}$). Upper abscissa: log spectral luminosity (W Hz^{-1}). Right ordinate: log weighted luminosity function $Jy^{1.5}$).

Since the shell model ignores local sources, it must fail at the highest flux densities - the regime in which a nonevolving model is more appropriate. What is surprising is that the transition flux density is so high. An exact calculation based on the same local luminosity function without evolution yields log $[S^{5/2}\, n(S \mid \nu = 1.4\ \text{GHz})] \approx 1.8$ at high flux densities (Figure 15.17), so the shell model and the nonevolving model predict the same source counts at $S \approx 20$ Jy. Thus, the static Euclidean approximation is reasonably good only for $S > 20$ Jy at $\nu = 1.4$ GHz; it applies only to the small number of sources in the very strongest flux-density bin plotted in Figure 15.17. It should not be used to describe features in the observed counts at lower flux densities. For example, the so-called "Euclidean" regions in which $S^{5/2}\, n(S \mid \nu = 1.4\ \text{GHz})$ is roughly constant near $\log[S(\text{Jy})] \approx 0$ and $\log[S(\text{Jy})] \approx -3$ do not indicate that the sources in these flux-density ranges are comparatively local - they only correspond to maxima in the visibility function of sources at $z \approx z_s$.

In the shell model, the median source redshift is $\langle z \rangle = z_s \approx 0.8$ for all $S << 20$ Jy, in good agreement with the observed redshift distribution of sources stronger than $S = 2$ Jy (Figure 15.9) and the magnitude distributions of galaxies identified with sources as faint as $S \approx 1$ mJy (Windhorst et al. 1984a, Kron et al. 1985). Since $\langle z \rangle$ is independent of S (no Hubble relation), there is a one-to-one correspondence between average luminosity and flux density that maps populations from the local visibility function to the weighted source count. Two consequences are as follows. (1) All standard evolutionary models (Section 15.5.2) require that the evolution function $E(L, z)$ be largest at high *luminosities*. The shell model reproduces this result (see Figure 15.1) because the difference between the weighted source counts observed and predicted by the nonevolving model are largest at high *flux densities*. (2) At any flux-density level, most sources will lie in a narrow range of luminosities; observations with that

sensitivity look beyond the shell for more luminous sources and will not reach the shell for less luminous ones. Deeper surveys do not detect more distant sources, only feebler ones. Consequently, elliptical galaxies account for nearly all of the strongest radio sources and spiral galaxies the faintest. There is a transition region at $S \approx 1$ mJy in which both populations should be present. Because the local visibility function is falling rapidly for luminosities $L < 10^{21}$ W Hz^{-1} this model also suggests that the (as yet unobserved) weighted source count will decline rapidly for flux densities $S < 10^{-5}$ Jy. [The widespread belief that nearby galaxies must eventually dominate the source count and cause its slope to approach the static Euclidean value is incorrect. Even with no evolution at all in an expanding universe, the slope of the weighted source count at low flux densities tends to approach that of the local visibility function at low luminosities (about 4/3 rather than zero); and most sources are cosmologically distant, crowding up against the redshift "cutoff" imposed by the $(1 + z)^{-9/4-3<\alpha>/2}$ term in Equation (15.30).]

Many authors have commented that the relatively narrow peak in the weighted source counts is difficult to model in terms of the relatively broad local luminosity function. It is inappropriate to compare these distributions because they do not have the same dimensions. The weighted source count $S^{5/2}n(S \mid \nu)$ should only be compared with the weighted local luminosity function $\phi(L \mid z = 0, \nu)$; the unweighted source count $n(S \mid \nu)$ is most appropriately compared with the unweighted local luminosity function $\rho(L \mid z = O, \nu)$. Figure 15.17 shows that the weighted source counts and the local visibility function peaks actually have very similar widths at $\nu = 1.4$ GHz. The only conclusion that can be drawn from the fact that the weighted source count peak is not much broader than the local visibility function peak is that *some* form of evolution is restricting the lower end of the redshift range $\Delta \log z$ in which most radio sources are found. [The factor $(1 + z)^{-9/4-3<\alpha>/2} = (1 + z)^{-3.3}$ for $<\alpha> = 0.7$ in Equation (15.30) is quite effective at suppressing the contribution of high-redshift sources to the observed source counts, so the success of the shell model is not strong evidence that evolution stops or reverses at redshifts higher than z_s.]

The very similar forms of the *local* visibility function and the weighted source count (Figure 15.17) determined by the visibility function at $z \approx 0.8$ indicate that the form of the visibility function really does not evolve significantly; i.e., the "translation evolution" approximation is a good one. Pure luminosity evolution works in the shell model, and pure density evolution in a thin shell would also preserve the form of the local visibility function in the normalized source counts. The amounts of luminosity and density evolution actually required to fit the data are determined by the redshift of the shell, the difference between the luminosity of the local visibility function peak and the flux density of the weighted count peak, and the difference between the peak values of the local visibility function and the weighted source count, as described above. Pure luminosity evolution shifts the source-count curve along a line of slope 3/2 in the $\{\log(S), \log[S^{5/2}\, n(S)]\}$-plane, and pure density evolution shifts it vertically. Thus, only one combination of luminosity and density evolution can match both z_m and the peak of weighted source count exactly.

The shell model emphasizes the insensitivity of the $<\theta>$ - S relation to source size evolution. Since there is no Hubble relation for $S << 20$ Jy, evolution of the projected linear size d with z affects sources of all flux densities equally. Furthermore, most sources with $S << 20$ Jy lie at redshifts within a factor of two

of $z_s = 0.8$, so they are at very nearly the same angular-size distance if $\Omega = 1$ (Figure 15.15). Thus the $<\theta>$ - S plot really measures the variation of projected linear size d with luminosity. The flat region with $<\theta> \approx 10$ arcsec extending from $S \approx 1$ mJy to $S \approx 1$ Jy indicates that $<d> \approx 40$ kpc for all luminosities in the range $L \approx 10^{24}$ to 10^{27} W Hz^{-1} at $\nu = 1.4$ GHz. The sudden falloff to $<\theta> < 3$ arcsec below $S \approx 1$ mJy cannot be caused by evolution; it reveals instead a dramatic decline in linear size to $<d> < 10$ kpc among sources less luminous than $L \approx 10^{24}$ W Hz^{-1}. Such a decline is expected if most of the sources contributing to the flattening of $S^{5/2}\, n(S \mid \nu)$ below $S \approx 1$ mJy at $\nu = 1.4$ GHz are in the disks of spiral galaxies.

15.10. WHAT NEXT?

(1) Despite our failure to find (or recognize) "standard candles" or "standard rods" relating L and S or d and θ, they would allow potentially definitive tests of world models and should not be forgotten. Every advance in instrumentation, every increase in astrophysical knowledge of radio sources should be considered an opportunity for determining world-model parameters. For example, recent high-sensitivity VLBI maps have found milliarcsecond jets with bulk relativistic velocities nearly equal to the speed of light, even in extended steep-spectrum sources whose orientations relative to the line of sight should be random. The angular separations between cores and jet knots in a complete sample of such sources might be combined with their nearly "standard velocities" $v \approx c$ to measure directly the angular-size distances corresponding to the source redshifts.

(2) The source counts $n(S \mid \nu)$ are generally better determined than most of the data needed for their interpretation. Little progress can be made at high flux densities because essentially the whole sky has been covered with accurate measurements. The sensitivity limits of the current generation of telescopes has nearly been reached. Source counts below $S \approx 10\mu$Jy at $\nu = 1.4$ GHz will be difficult to obtain directly, although some limits to the source counts at fainter levels might be obtained from background measurements. Increasing the sky area covered by deep surveys is still needed to reduce the statistical errors, especially at $\nu = 5$ GHz, where each map only covers about 10^{-5} steradians. Overlapping surveys at 1.4 and 5 GHz are badly needed to determine the spectral-index distributions of faint sources selected at these two frequencies.

(3) The weighted local luminosity function at $\nu = 1.4$ GHz has larger statistical errors than the weighted source count, particularly near the peaks of the spiral-galaxy and elliptical-galaxy contributions, so it contributes significantly to the uncertainty in the evolution function $E(L, z)$. Improvements are especially needed near $L \approx 10^{23}$ W Hz^{-1} at $\nu = 1.4$ GHz to interpret the source count near $S \approx 1$ mJy and decide whether a "new population" of sources exists. This will require an optically complete sample with known redshifts filling a large volume of space; the UGC sample (Nilson 1973) for example. Radio observations of the same sample should be made at $\nu = 5$ GHz as well as at a lower frequency so that the local luminosity functions of steep- and flat-spectrum sources can be determined independently.

(4) Redshifts of complete samples of flat-spectrum sources stronger than $S \approx 0.1$ Jy should be measured to confirm suggestions that evolution peaks at $z \approx 2$. This may not be too difficult because most flat-

spectrum sources stronger than $S \approx 0.1$ Jy can be identified with fairly bright quasars with strong emission lines. If very-high-redshift quasars are common, they will surely be found in such samples. If they are not, only radio-selected samples may be sufficiently immune to selection effects to prove it.

(5) Optical programs like the Leiden-Berkeley Deep Survey should be extended to sources as faint as $S \approx 0.1$ mJy at $\nu = 1.4$ GHz to determine the redshift distribution and host galaxy population of the faint-source population.

(6) High-resolution ($\approx 1''$) maps of sources fainter than $S \approx 1$ mJy should also be made to determine their angular-size distributions and improve their radio positions for reliable optical identifications.

(7) Isotropy tests at somewhat higher effective resolutions should be made to detect density fluctuations on scales less than 50 Mpc.

Recommended Reading

Annual Review Article

Jauncey D.L. (1975). Radio Surveys and Source Counts, Annu. Rev. Astron. Astrophys. 13:23.

Books

Maeder A., Martinet L., and G. Tammann, eds. 1978. Observational Cosmology. Geneva: Geneva Observatory.

Sandage A., Sandage M., and J. Kristian, eds. 1975. Galaxies and the Universe. Chicago: University of Chicago Press.

Symposia Proceedings

Jauncey D.L., ed. 1977. Radio Astronomy and Cosmology. Proc. I.A.U. Symposium 74.

Hewitt A., Burbidge G., and Li-Zhi Fang, eds. 1987. Observational Cosmology. Proc. I.A.U. Symposium 124.

REFERENCES

1. Allington-Smith, J.R. 1984. Mon. Not. R. Astron. Soc. 210:611.
2. Auriemma, C., G.C. Perola, R. Ekers, R. Fanti, C. Lari, W.J. Jaffe, and M.H. Ulrich. 1977. Astron. Astrophys. 57:41.
3. Bahcall, N.A., and W.S. Burgett. 1986. Astrophys. J. 300:L35.

4. Biermann, P., A. Eckart, and A. Witzel. 1985. Astron. Astrophys. 142:L23.
5. Bridle, A.H. 1967. Mon. Not. R. Astron. Soc. 136:219.
6. Coleman, P.H. 1985. Ph.D. thesis, University of Pittsburgh.
7. Coleman, P.H., and J.J. Condon. 1985. Astron. J. 90:1431.
8. Coleman, P.H., J.J. Condon, and C. Hazard. 1985. Astron. J. 90:1437.
9. Condon, J.J. 1974. Astrophys. J. 188:279.
10. Condon, J.J. 1984a. Astrophys. J. 284:44.
11. Condon, J.J. 1984b. Astrophys. J. 287:461.
12. Condon, J.J. 1987. Astrophys. J. Suppl. 65, in press.
13. Condon, J.J., and J.J. Broderick. 1985. Astron. J. 90:2540.
14. Condon, J.J., and J.J. Broderick. 1986. Astron. J. 92:94.
15. Condon, J.J., M.A. Condon, G. Gisler, and J.J. Puschell. 1982a. Astrophys. J. 252:102.
16. Condon, J.J., M.A. Condon, and C. Hazard. 1982b. Astron. J. 87:739.
17. Condon, J.J., and J.E. Ledden. 1981. Astron. J. 86:643.
18. Crawford, D.F., D.L. Jauncey, and H.S. Murdoch. 1970. Astrophys. J. 162:405.
19. Danese, L., G. De Zotti, and N. Mandolesi. 1983. Astron. Astrophys. 121:114.
20. de Lapparent, W., M.J. Geller, and J.P. Huchra. 1986. Astrophys. J. 302: Ll.
21. Downes, A.J.B., M.S. Longair, and M.A.C. Perryman. 1981. Mon. Not. R. Astron. Soc. 197:593.
22. Ellis, G.F.R., and J.E. Baldwin. 1984. Mon. Not. R. Astron. Soc. 206:377.
23. Fanaroff, B.L., and M.S. Longair. 1973. Mon. Not. R. Astron. Soc. 161:393.
24. Fielden, J., A.J.B. Downes, J.R. Allington-Smith, C.R. Berm, M.S. Longair, and M.A.C. Perryman. 1983. Mon. Not. R. Astron. Soc. 204:289.
25. Fomalont, E.B., A.H. Bridle, and M.M. Davis. 1974. Astron. Astrophys. 36:273.
26. Fomalont, E.B., K.I. Kellermann, J.V. Wall, and D. Weistrop. 1984. Science 225:23.
27. Grueff, G., and M. Vigotti. 1977. Astron. Astrophys. 54:475.
28. Hacking, P., J.J.- Condon, and J.R. Houck. 1987. Astrophys. J. 316:L15.
29. Hooley, A., M.S. Longair, and J.M. Riley. 1978. Mon. Not. R. Astron. Soc. 182:127.
30. Hughes, R.G., and M.S. Longair. 1967. Mon. Not. R. Astron. Soc. 135:131.
31. Jauncey, D.L. 1967. Nature 216:877.
32. Jauncey, D.L. 1975. Annu. Rev. Astron. Astrophys. 13:23.
33. Kapahi, V.K. 1975. Mon. Not. R. Astron. Soc. 172:513.
34. Kapahi, V.K. 1985. Mon. Not. R. Astron. Soc. 214:19P.
35. Kapahi, V.K. 1986. In Proc. Int. Astron. Union Symp. 124. A. Hewitt, G. Burbidge, and L.Z. Fang (eds.), Dordrecht: Reidel, p. 251.
36. Kapahi, V.K., and C.R. Subrahmanya. 1982. In Proc. Int. Astron. Union. Symp. 97. D.S. Heeschen and C.M. Wade (eds.), Dordrecht: Reidel, p. 401.
37. Kapahi, V.K., V.K. Kulkarni, and C.R. Subrahmanya. 1987. J. Astrophys. Astron. 8:33.
38. Kellermann, K.I. 1964. Astrophys. J. 140:969.
39. Kellermann, K.I. 1972. Astron. J. 77:531.
40. Kron, R.G., D.C. Koo, and R.A. Windhorst. 1985. Astron. Astrophys. 146:38.
41. Kühr, H., A. Witzel, I.I.K. Pauliny-Toth, and U. Nauber. 1981. Astron. Astrophys. Suppl. 45:367.
42. Kulkarni, V.K. 1978. Mon. Not. R. Astron. Soc. 185:123.
43. Laing, R.A., and J.A. Peacock 1980. Mon. Not. R. Astron. Soc. 190:903.

44. Laing, R.A., J.M. Riley, and M.S. Longair 1983. Mon. Not. R. Astron. Soc. 204:151.
45. Longair, M.S. 1966. Mon. Not. R. Astron. Soc. 133:421.
46. Longair, M.S. 1978. In Observational Cosmology. A. Maeder, L. Martinet, and G. Tammann (eds.), Geneva: Geneva Observatory, p. 125.
47. Longair, M.S., and P.A.G. Scheuer. 1970. Mon. Not. R. Astron. Soc. 151:45.
48. Longair, M.S., and M. Seldner. 1979. Mon. Not. R. Astron. Soc. 189:433.
49. Machalski; J. 1977. Astron. Astrophys. 56:53.
50. Machalski, J. 1978. Astron. Astrophys. 65:157.
51. Machalski, J. 1981. Astron. Astrophys. Suppl. 43:91.
52. Maslowski, J., J. Machalski, and S. Zieba. 1973. Astron. Astrophys. 28:289.
53. Masson, C. 1979. Mon. Not. R. Astron. Soc. 188:261.
54. Mattig, W. 1958. Astron. Nachr. 284:109.
55. Meiksin, A., and M. Davis. 1986. Astron. J. 91:191.
56. Meurs, E.J.A., and A.S. Wilson. 1984. Astron. Astrophys. 136:206.
57. Miley, G.K. 1971. Mon. Not. R. Astron. Soc. 152:477.
58. Mitchell, K.J. 1983. Ph.D. thesis, Pennsylvania State University.
59. Mitchell, K.J., and J.J. Condon 1985. Astron. J. 90:1957.
60. Nilson, P. 1973. Uppsala General Catalogue of Galaxies. Uppsala: Uppsala Astronomical Observatory.
61. Oort, M.J.A. 1987. Astron. Astrophys., submitted
62. Oort, M.J.A., P. Katgert, F.W.M. Steeman, and R.A. Windhorst 1987. Astron. Astrophys. 179:41.
63. Ostriker, J.P., and J. Heisler. 1984. Astrophys. J. 278:1.
64. Owen, F.N., J.J. Condon, and J.E. Ledden. 1983. Astron. J. 88:1.
65. Pauliny-Toth, I.I.K., A. Witzel, E. Preuss, H. Kiihr, K.I. Kellermann, E.B. Fomalont, and M.M. Davis. 1978. Astron. J. 83:451.
66. Peacock, J.A. 1985. Mon. Not. R. Astron. Soc. 217:601.
67. Peacock, J.A., and S.F. Gull. 1981. Mon. Not. R Astron. Soc. 196:611.
68. Petrosian, V., and J. Dickey. 1973. Astrophys. J. 186:403.
69. Pfleiderer, J. 1977. Astron. Astrophys. Suppl. 28:313.
70. Rees, M.J., and G. Setti. 1968. Nature 219:127.
71. Robertson, J.G. 1973. Aust. J. Phys. 26:403.
72. Robertson, J.G. 1978. Mon. Not. R. Astron. Soc. 182:617.
73. Robertson, J.G. 1980. Mon. Not. R. Astron. Soc. 190:143.
74. Rowan-Robinson, M. 1970. Mon. Not. R. Astron. Soc. 149:365.
75. Rowan-Robinson, M., D. Walker, T. Chester, T. Soifer, and J. Fairclough. 1986. Mon. Not. R. Astron. Soc. 219:273.
76. Ryle, M., and R.W. Clarke. 1961. Mon. Not. R. Astron. Soc. 122:349.
77. Sandage; A. 1961. Astrophys. J. 133:355.
78. Sandage, A., and G.A. Tammann 1981. A Revised Shapley-Ames Catalog of Bright Galaxies. Washington, D.C.: Carnegie Institute of Washington.
79. Scheuer, P.A.G. 1957. Proc. Cambridge Phil. Soc. 53:764.
80. Scheuer, P.A.G. 1974. Mon. Not. R. Astron. Soc. 166:329.
81. Schmidt, M. 1968. Astrophys. J. 151:393.

82. Schmidt, M. 1972. Astrophys. J. 176:303.
83. Schmidt, M. 1976. Astrophys. J. 209:L55.
84. Spinrad, H., S. Djorgovski, J. Marr, and L. Aguilar. 1985. Publ. Astron. Soc. Pacific 97:932.
85. Subrahmanya, C.R., and V.K. Kapahi. 1983. G.O. Abell and G. Chincarini (eds.), Proc. Int. Astron. Union Symp. 104. Dordrecht: Reidel, p. 47.
86. Terrell, J. 1977. Am. J. Phys. 45:869.
87. van der Laan, H., and R.A. Windhorst. 1982. H.A. Briick, G.V. Coyne, and M.S. Longair (eds.), Astrophysical Cosmology. Vatican City: Pontificia Academia Scientiarum, p. 349.
88. Véron-Cetty, M.P., and P. Véron. 1983. Astron. Astrophys. Suppl. 53:219.
89. von Hoerner, S. 1973. Astrophys. J. 186:741.
90. Wall, J.V., and J.A. Peacock. 1985. Mon. Not. R Astron. Soc. 216:173.
91. Walls, J.V., T.J. Pearson, and M.S. Longair. 1980. Mon. Not. R. Astron. Soc. 193:683.
92. Wall, J.V., C.R. Bern, G. Grueff, and M. Vigotti. 1986. J.-P. Swings (ed.), Highlights of Astronomy. Dordrecht: Reidel, p. 345.
93. Webster, A. 1976a. Mon. Not. R. Astron. Soc. 175:6t.
94. Webster, A. 1976b. Mon. Not. R. Astron. Soc. 175:71.
95. Weistrop, D., J.V. Wall, E.B. Fomalont, and K.I. Kellermann. 1987. Astron. J. 93:805.
96. Windhorst, R. 1984. Ph.D. thesis, University of Leiden.
97. Windhorst, R. 1986. J. P. Swings (ed.), Highlights of Astronomy. Dordrecht: Reidel, p. 355.
98. Windhorst, R., R.G. Kron, and D.C. Koo. 1984a. Astron. Astrophys. Suppl. 58:39.
99. Windhorst, R., G.M. van Heerde, and P. Katgert. 1984b. Astron. Astrophys. Suppl. 58:1.
100. Windhorst, R., G.K. Miley, F.N. Owen, R.G. Kron, and D.C. Koo. 1985. Astrophys. J. 289:494.
101. Witzel, A., J. Schmidt, I.I.K. Pauliny-Toth, and U. Nauber. 1979. Astron. J. 84:942.